A Fourier Transform Infrared trace gas analyser for atmospheric applications

David W. T. Griffith[1]*, Nicholas M. Deutscher[1,2], Christopher Caldow[1], Graham Kettlewell[1], Martin Riggenbach[1] and Samuel Hammer[3]

[1]University of Wollongong, Wollongong NSW 2522, Australia

[2] Now at University of Bremen, Institute of Environmental Physics, Bremen, Germany

[3] University of Heidelberg, Institute of Environmental Physics, Heidelberg, Germany

Keywords:

Atmospheric trace gas analysis, Fourier transform spectroscopy, FTIR, carbon dioxide, methane, carbon monoxide, nitrous oxide, carbon isotopes, water isotopes, micrometeorological flux measurements, flux chamber

Revised manuscript (August 2012) for Atmospheric Measurement Techniques, GGMT special issue, April 2012.

* corresponding author, griffith@uow.edu.au

Abstract

Concern in recent decades about human impacts on Earth's climate has led to the need for improved and expanded measurement capabilities for greenhouse gases in the atmosphere. In this paper we describe in detail an in situ trace gas analyser based on Fourier Transform Infrared (FTIR) spectroscopy that is capable of simultaneous and continuous measurements of carbon dioxide (CO_2), methane (CH_4), carbon monoxide (CO), nitrous oxide (N_2O) and ^{13}C in CO_2 in air with high precision. High accuracy is established by reference to measurements of standard reference gases. Stable water isotopes can also be measured in undried airstreams. The analyser is automated and allows unattended operation with minimal operator intervention. Precision and accuracy meet and exceed the compatibility targets set by the World Meteorological Organisation – Global Atmospheric Watch for baseline measurements in clean air for all species except ^{13}C in CO_2.

The analyser is mobile and well suited to fixed sites, tower measurements, mobile platforms and campaign-based measurements. The isotopic specificity of the optically-based technique and analysis allows application in isotopic tracer experiments, for example in tracing variations of ^{13}C in CO_2 and ^{15}N in N_2O. We review a number of applications illustrating applications of the analyser in clean air monitoring, micrometeorological flux and tower measurements, mobile measurements on a train, and soil flux chamber measurements.

1. Introduction

Growing concern in recent decades about human impacts on Earth's climate has led to the need for improved understanding of greenhouse gases in the atmosphere and the global carbon cycle. The Fourth Assessment Report of the Intergovernmental Panel on Climate Change (IPCC, 2007) provides the most recent and extensive overview of the physical basis of human-induced climate change. Carbon dioxide (CO_2) and methane (CH_4) are the most important anthropogenic long lived greenhouse gases (GHGs), accounting for 64% and 18% of human-induced radiative forcing respectively (Hofmann et al., 2006, for update see http://www.esrl.noaa.gov/gmd/aggi/). Nitrous oxide (N_2O) follows the chlorofluorcarbons F-11 ($CFCl_3$) and F-12 (CF_2Cl_2) with a 4%, contribution that is increasing as the now-restricted chlorofluorocarbons decay in the atmosphere in coming decades (Ravishankara et al., 2009). Major sources of anthropogenic CO_2 increases are fossil fuel combustion for energy; for CH_4 they are increased wetlands and agricultural livestock emissions, and for N_2O the increased use of nitrogeneous fertilisers in agriculture. CO_2 emissions are partially taken up and recycled by the oceans, land and the biosphere, but approximately half of fossil fuel CO_2 accumulates in the atmosphere. CH_4 and N_2O are ultimately chemically destroyed in the atmosphere, but increasing sources also mean that their atmospheric abundances are increasing (IPCC, 2007).

Measurements of greenhouse gases in the atmosphere provide the fundamental data on which our understanding is based. In situ measurements at the local or ecosystem level lead to "bottom-up" detailed understanding of the individual processes and magnitudes of GHG exchanges, but are necessarily sparse and require significant up-scaling and extrapolation to be used in global-scale models of GHG source-sink distributions and inventories. In the alternative "top-down" approach, time series of in situ and remote sensing measurements are combined with inverse models and atmospheric transport to infer source-sink distributions at global scales, but here the problem is mathematically ill-posed, and uncertainties are dominated by the sparseness of the available measurements. Both top down and bottom up approaches benefit from new techniques which can increase the density and accuracy of available measurements. In particular, the extension of measurements from occasional, often flask-based sampling programmes to continuous measurements near the ground, on tall towers, and from satellites is highly desirable. Continuous measurements resolve variability on diurnal and synoptic timescales which can be increasingly resolved by higher resolution models. However the accuracy requirements are stringent – the World Meteorological Organisation's Global Atmospheric Watch (GAW) specifies the required inter-station compatibility and lack of bias required for measurements to

improve understanding of global greenhouse gas cycling. These requirements and approximate global mean atmospheric mole fractions (2010) are listed in Table 1 (GAW, 2011)

Regular atmospheric GHG measurements effectively began in the International Geophysical Year of 1957 with the establishment of CO_2 measurements by non dispersive infrared spectroscopy (NDIR) at Mauna Loa in Hawaii by C. D. Keeling (Keeling et al., 1995), and are now continuous at several global sites (e.g. Francey et al., 2010; Steele et al., 2011, see also http://www.esrl.noaa.gov/gmd/). For other species, high accuracy greenhouse gas measurements have been dominated by gas chromatography (GC) techniques using various detectors. GC requires frequent calibration but can be automated and is commonly used to provide pseudo-continuous spot-measurements for most species in many stations and networks (see for example (van der Laan et al., 2009; Vermeulen et al., 2011; Popa et al., 2010; Prinn et al., 2000; Langenfelds et al., 2011).

Optical techniques based on the absorption or emission of radiation are well suited to continuous measurements and have a robust physical basis for calibration. Recent advances in laser-based techniques have achieved the required precision in many cases and several instruments have become commercially available. Lasers are inherently single-wavelength devices that can be scanned over single absorption lines in a narrow wavelength interval. They are typically restricted to only one or two species, but high brightness of the laser source leads to low noise and high precision measurements. Earlier instruments used liquid nitrogen-cooled lead-salt mid-IR lasers ($\lambda > 2.0$ μm), but these have been largely supplanted by cheaper, mass produced and readily available near-IR ($\lambda \sim 0.7 – 2.0$ μm) lasers sourced from the telecommunications industry and operating near room temperature. While the near-IR lasers are relatively cheap and freely available, absorption bands in the near-IR are generally overtone and combination bands which are weak absorbers compared to the fundamental vibration bands in the mid-IR. The weak absorption cancels some of the advantage of high brightness and low noise, and long absorption paths are required to obtain the desired precision. Most recently, quantum cascade lasers operating near room temperature at mid-IR wavelengths have been developed, and these are becoming commercially available (e.g.Tuzson et al., 2011).

Fourier Transform InfraRed (FTIR) spectroscopy offers an alternative infrared optical technique to laser spectroscopy. FTIR uses broadband infrared radiation from a blackbody light source that covers the entire infrared spectrum simultaneously. In FTIR spectroscopy the source radiation is modulated by a Michelson interferometer and all optical frequencies are recorded simultaneously in the measured interferogram (Davis et al., 2001; Griffiths and de Haseth, 2007). A

mathematical Fourier transform retrieves the spectrum (intensity vs frequency) from the interferogram. Compared to laser sources the blackbody source is less bright, but this disadvantage is largely offset by the multiplex advantage of measuring the whole spectrum simultaneously, and operation in the mid-IR region where absorption bands are strong compared to the near-IR. The result is precision similar to or better than NIR-laser based instruments, but with the ability to determine several species, including isotopologues, simultaneously from the same measured spectrum.

Figure 1 shows the mid infrared spectra of whole clean air, dried and undried, in a 24 m path absorption cell as recorded with the analyser described in this paper. The target gases, carbon dioxide (CO_2) methane (CH_4), nitrous oxide (N_2O), carbon monoxide (CO), and water vapour (H_2O) have absorption bands in this region. Infrared absorption frequencies depend on the atomic masses, and in the case of $^{13}CO_2$ the ν_3 stretching vibration is shifted 66 cm^{-1} from the parent $^{12}CO_2$ band, which allows independent determination of ^{13}C composition in CO_2 with a low resolution FTIR spectrometer. H^2HO (HDO) absorption is also well separated from that of H_2O and allows measurements of H/D fractionation (Parkes et al., 2012). Quantitative analysis of broad regions of the spectrum (typically 100-200 cm^{-1} wide) including whole absorption bands of the molecules of interest provides the concentrations of the target species. The spectral information from many ro-vibronic lines is included in each analysis, enhancing the information content of the measurement compared to narrow-band, single line laser methods, thus leading to high measurement precision and stability.

In this paper we describe the construction, performance and selected applications of a high precision trace gas analyser based on low resolution Fourier Transform Infrared (FTIR) spectrometry. The FTIR spectrometer is coupled to a multi-pass (White) cell and a gas sampling manifold and is principally intended for in situ sampling and analysis of ambient air. The analyser is fully automated and provides real-time concentration or mole fraction measurements of target gases including CO_2, CO, CH_4, N_2O, H_2O and the isotopologues $^{13}CO_2$, HDO and $H_2{}^{18}O$. The analyser is an extension of earlier work (Esler et al., 2000a, b) and incorporates significant improvements in usability and performance. Parkes et al. describe optimisation of the analyser for stable water isotope measurements (Parkes et al., 2012).

2. Description of the analyser

The FTIR spectrometer is a Bruker IRcube, a modular unit built around a frictionless flex-pivot interferometer with 1 cm^{-1} resolution (0.5 cm^{-1} optional) and 25 mm beam diameter, globar

source and CaF_2 beamsplitter. The modulated exit beam is coupled to a multipass White cell by transfer optics consisting of two flat mirrors. The White cell is a permanently aligned glass cell, f-matched to the FTIR beam with a total folded path of 24 m and volume 3.5 L. The beam exiting the White cell is directed back into the IRcube and focussed onto a 1 mm diameter thermoelectrically-cooled MCT detector with peak detectivity at 2000 cm^{-1}. The interferometer is scanned at 80 scans min^{-1} and normally spectra are coadded for 1-10 min according to the required time resolution and signal-to-noise ratio. The root mean square (RMS) signal-to-noise ratio in the spectra for a 1-minute average measurement (80 coadded spectra) through the cell at 1 cm^{-1} resolution is typically 40,000-60,000:1 (measured as 1/noise where noise is the rms noise from 2500-2600 cm^{-1} on the ratio of two consecutively collected spectra). The signal-to-noise ratio (SNR) increases as the square root of averaging time for coadded spectra up to at least 20 minutes.

The White cell is fitted with a 0-1333 hPa piezo-manometer to measure cell pressure and a type-J or type-T thermocouple in the cell for cell temperature measurement. Ambient water vapour, CO_2, CO, CH_4 and N_2O are removed from the internal volume of the IRcube and transfer optics with a slow purge of dry N_2 (0.1-0.2 L min^{-1}) backed by a molecular sieve and Ascarite® trap in the volume. The FTIR and sample cell are thermostatted, typically at 30ºC.

The evacuation and filling of the cell with sample or calibration gas is controlled by a manifold of solenoid valves, shown schematically in Figure 2. A 4-stage oil-free diaphragm pump with ultimate vacuum of approximately 1 hPa is used to evacuate and draw sample gas through the cell. Sample or calibration gas streams are introduced through one of four equivalent inlets (V1-V4). To minimise uncertainty due to cross-sensitivity to water vapour lines in the spectra (section 3), the airstream can be optionally dried by passing through a Nafion® drier and $Mg(ClO_4)_2$ trap (selected by V9). The gas stream passes through a 7 µm sintered stainless steel particle filter into the sample cell (V6). Flow is controlled by a mass flow controller which can optionally function as a cell pressure controller through a feedback loop to the cell pressure transducer. In earlier versions of the analyser, a needle valve and mass flow meter were used instead of the mass flow controller. In the most recent versions, the addition of a second mass flow controller upstream of the cell (not shown) allows both pressure and flow to be controlled simultaneously. Flow rate is typically 0.5 – 1.5 L min^{-1} and cell pressure near ambient pressure. The dried sample gas stream leaving the cell provides the required backflush to the Nafion dryer at reduced pressure. The Nafion drier alone typically achieves water vapour mole fractions of 200-300 µmol mol^{-1} (dew point <-40ºC) in the sampled airstream, and the $Mg(ClO_4)_2$ typically

reduces this to < 10 μmol mol^{-1}. Sample or calibration gas may also be analysed statically by evacuating and filling the cell without flow during the measurement. In this case a flow of dried air can be maintained through the Nafion drier via a cell-bypass valve (V5) to avoid step changes in water vapour levels which may occur if the Nafion drier is not continuously flushed. The cell can be evacuated directly through V8.

The solenoid manifold valves are switched by a digital output (DO) relay module connected to the controlling computer via a RS232-RS485 serial interface. An 8-channel, 16-bit analogue-digital converter (ADC) module is connected via the same RS485 daisy-chain to log pressure, cell and room temperatures, flow and other desired analogue signals. The mass flow controller is controlled by an analogue output (AO) module. Additional DO, AO or ADC modules can be added as required to the RS485 daisy chain for special applications. Operation of the spectrometer, sample manifold, data logging, spectrum analysis (described below) and real time display of gas concentrations is controlled by a single program ("Oscar") written in Microsoft Visual Basic. The spectrometer communication is via Bruker's OPUS DDE interface over a private Ethernet network. The DO, AO and ADC modules are connected via the PC's serial RS232 port. Oscar provides for the configuration and fully automated execution of user-defined sequences of valve-switching for flow control, spectrum collection, spectrum quantitative analysis, logging and display. Different sequences may be executed in turn and looped to provide continuous automated operation, including periodic calibration tank measurements, without manual intervention. The instrument can be run remotely via an ethernet connection to the PC.

Quantitative spectrum analysis

Spectra are analysed to determine the amounts of selected trace gases in the cell by non-linear least squares fitting of broad regions (100-200 cm^{-1}) of the spectrum selected for each target gas. The analysis is carried out automatically after spectrum collection, and the results logged and displayed on the controlling computer. Spectroscopic analysis fundamentally determines the total absorber amount (concentration x pathlength, $C \times L$) of the target trace gas, from which the mole fraction χ of the trace gas in air is calculated from the molar concentration of air, $n/V=P/RT$

$$\chi = \frac{C}{P/RT} \qquad \text{Eq. (1)}$$

where P is the measured sample pressure, T the sample cell temperature, and R the universal gas constant. From Eq. (1), χ is the mole fraction in whole air – χ can be converted to dry air mole

fraction using the measured mole fraction of water vapour in the sampled air in the cell determined simultaneously from the FTIR spectrum as in Eq. (2)

$$\chi_{dry} = \frac{\chi}{(1-\chi_{H2O})} \qquad \text{Eq. (2)}$$

For dried air χ_{H2O} is generally small (< 10 μmol mol^{-1}) and the correction to dry air mole fraction is negligible. The quantitative spectrum analysis takes a computational approach in which the spectral region to be analysed is iteratively fitted with a calculated spectrum. The spectrum model, MALT (Multiple Atmospheric Layer Transmission), and non-linear least squares retrieval of concentrations from spectra, are described in detail elsewhere (Griffith, 1996; 2012) and only summarised here. For most trace gases of interest, the positions, strengths, widths and temperature dependences of relevant absorption lines are available in the HITRAN database (Rothman et al., 2005). From the HITRAN line parameters, the MALT spectral model calculates the absorption coefficients of the gas sample in the cell at the measured temperature and pressure. For samples containing gases that are not included in HITRAN, the absorption coefficients can be calculated from quantitative library reference spectra if available – for example, the Northwest Infrared Vapour Phase Reference Library provides such data for over 400 compounds (https://secure2.pnl.gov/nsd/nsd.nsf/Welcome, see also (Sharpe et al., 2004; Johnson et al., 2010). The monochromatic (ie true, infinite resolution) transmittance spectrum is calculated from the absorption coefficients and initial estimates of trace gas concentrations, then convolved with the FTIR instrument lineshape (ILS) function, which includes the effects of resolution (maximum optical path difference of the interferogram), apodisation, and finite field of view (beam divergence in the interferometer). In addition, effects of imperfect alignment or optics can be included, for example wavenumber scale shift, loss of modulation efficiency at high optical path difference, and residual phase error, which may lead to shifted, broadened and asymmetric lineshapes respectively. The resulting calculated spectrum simulates the measured spectrum, and is iteratively re-calculated using a Levenberg-Marquardt algorithm (Press et al., 1992) to update estimates of absorber amounts and ILS parameters until the best fit (minimum sum of squared residuals between measured and calculated spectra) is achieved.

The transmittance model is not linear in the fitted parameters (absorber amounts and ILS), necessitating the iterative non-linear least squares fitting. This method is fundamentally different from methods commonly used in chemometric approaches to quantitative spectrum analysis, and in particular the Classic Least Squares (CLS) or Partial Least Squares (PLS) used in earlier work (Griffith, 1996). These chemometric approaches are applied to absorbance spectra and fit the

spectrum as a linear combination of single component absorbance spectra (CLS) or factors (PLS). They inherently assume that Beer's Law (i.e. that absorbance is proportional to concentrations of absorbers) is obeyed or nearly obeyed, but cannot fit spectral variations due to ILS effects, and are restricted to regions of weak absorption to avoid non-linearities and breakdown of Beer's Law (Anderson and Griffiths, 1975; Haaland, 1987). In non-linear least squares the transmittance spectrum can be fitted in any region, not just one of weak absorption, because there is no assumption of linearity between transmittance and trace gas concentrations. All spectral points have the same measurement noise error independent of the transmittance, and therefore have equal weight in calculating and minimising the residual sum of squares.

The iterative fit normally takes 5-10 iterations and a few seconds of computation time on a typical personal computer. Figure 3 illustrates spectral fits to typical regions: (a) 2150-2310 cm^{-1} for CO_2 isotopologues, CO and N_2O, (b) 2097 – 2242 cm^{-1} optimised for N_2O and CO (c) 3001 - 3150 cm^{-1} for CH_4, and (d) 3520-3775 cm^{-1} for CO_2 (all isotopologues) and H_2O. Water vapour is fitted in all spectral regions because there are weak residual water vapour lines even in dried air. In undried air, H_2O, HDO and $H_2{}^{18}O$ in the sample can be independently determined to provide the hydrogen and oxygen isotope composition in water vapour (Parkes et al., 2012, not shown). In the region near 2300 cm^{-1} the ^{13}C and ^{12}C isotopologues of CO_2 are well resolved (the $^{13}CO_2$ asymmetric stretching band is shifted 66 cm^{-1} from the corresponding $^{12}CO_2$ band) and can be fitted independently, allowing a direct measurement of ^{13}C composition in atmospheric CO_2. In general, overlap of absorption bands of different gases is accounted for by the MALT spectral model and isolated spectral features are not required for analysis. However cross-sensitivities may be significant with overlap of a weak band by a much stronger band, such as is the case for N_2O and $^{13}CO_2$ shown Figure 3(a) – in this case an additional window from 2097-2242 cm^{-1} shown in Figure 3(b) can be used to minimise this cross-sensitivity.

All spectra are stored after measurement and archived. An advantage of the method is that spectra can be re-analysed at any later time, for example with a different choice of spectral regions or with improved line parameters as they may become available.

The fitting procedure provides trace gas amounts and ILS parameters without any reference to calibration spectra of reference gases. For an ideal measured spectrum from a perfectly aligned spectrometer, the fitted spectrum residual should show only random detector noise and absolute accuracy would depend only on the HITRAN line parameters, pressure, temperature and pathlength measurements. In reality, the raw FTIR determination of trace gas concentrations is highly precise, but typically accurate only to within a few percent due to systematic errors in the

spectrometer, MALT model, HITRAN data and measured pressure and temperature (Smith et al., 2011). Higher accuracy, equivalent to the precision of repeated measurements, is achieved by analysis of calibration standards that have known concentrations traceable to accepted standard scales such as the WMO scales for clean air (GAW, 2011). Calibration equations can be derived by analysis of one or more such standards. Details of precision and accuracy are given in the following section.

The analyser and spectral analysis procedure has been developed and improved over several years since the first versions described by Esler et al. (2000a, b). Since 2011 the analyser described above, with refinements, is available commercially as the Spectronus analyser from Ecotech Pty Ltd., Knoxfield, Australia.

3. Precision, accuracy and calibration

Precision

Precision may be quantified as *repeatability* (the closeness of the agreement between the results of successive measurements of the same measurand carried out under the same conditions of measurement) or *reproducibility* (where the conditions of measurement may include different operators, locations and techniques). *Accuracy* is defined as the closeness of the agreement between the result of a measurement and a true value of the measurand (JCGM, 2008, see also http://gaw.empa.ch/glossary.html).

Repeatability of the FTIR analyser is determined as the standard deviation of replicate measurements of a gas sample of constant composition, for example a set of measurements of a constant air sample in the sample cell. Figure 4 illustrates the analyser's repeatability with time series (upper panels) and Allan deviation (lower panels) of consecutive 1-minute measurements of CO_2, CH_4, CO, N_2O and $\delta^{13}C$ in CO_2 in dry air. For these measurements the cell was slowly flushed with dried air from a high pressure tank, and spectra collected continuously for more than 2 days (54 hours). Pressure in the cell was controlled at 1100 hPa.

Allan variance is commonly used to characterise noise in repeated measurements (Allan, 1966; Werle et al., 1993) and expresses the measurement variance as a function of averaging time. In Figure 4 the plotted Allan deviation is the square root of the Allan variance. If the variance is dominated by white (Gaussian) noise, as should occur in the ideal case when the precision is detector noise limited, the Allan variance should decrease linearly with averaging time and the log plots of Allan deviation in Figure 4 should have slope of -0.5, as indicated by the dotted

lines. From Figure 4 it can be seen that in most cases the Allan deviation decreases with $\sqrt{time}$ for at least 30 minutes. Repeatabilities (as Allan deviations) for averaging times of 1 and 10 minutes are summarised in Table 1. These repeatabilities meet GAW compatibility requirements for baseline air monitoring (also listed in Table 1) for all species except $\delta^{13}C$ in CO_2.

Calibration and accuracy

The least squares fitting of spectra provides trace gas concentrations for which the absolute accuracy depends on the FTIR instrument response, HITRAN line parameters, the MALT spectrum model and the accuracy of the least squares fitting procedure. The raw "FTIR" mole fraction scale also includes measurements of sample pressure and temperature (Eq. (1)) and their associated uncertainties. The raw FTIR measurements are *precise* as described above, but absolute *accuracy* is typically less, up to a few percent (Griffith, 2012; Smith et al., 2011). Calibration of the analyser to an absolute or reference scale is achieved by measurements of two or more tanks of air independently calibrated for each trace gas on the reference scales. Calibration is described in detail in an accompanying paper by Hammer et al. (2012) and shown to exceed GAW compatibility targets (Table 1) for accuracy for all species except $\delta^{13}C$ in CO_2. Griffith et al. (2011) and Hammer et al., (2012) demonstrate that the raw FTIR scale is linear relative to WMO reference scales over a range of mole fractions typical of ambient air and above. While the calibration regressions are in general linear within the measurement error limits, they have small but significant non-zero y-axis intercepts, so the general calibration equation for each species is expressed as

$$\chi_{meas} = a.\chi_{ref} + b \qquad \text{Eq. (3)}$$

where a and b are the coefficients derived from slope and intercept of the regression.

Figure 5 shows residuals from linear regressions of FTIR-measured mole fractions against reference values from a suite of standard tanks maintained at the University of Heidelberg (data from Hammer et al., 2012). Similar measurements over wider mole fraction ranges for a suite of tanks at CSIRO's GASLAB also show no significant deviations from linearity (albeit with lower precision) (Griffith et al., 2011). Possible effects of small non-linearities are observed in the calibration of $\delta^{13}C$ in CO_2 measurements, described below.

Calibration stability

The Allan variance plots of Figure 4 (upper panels) illustrate the uncalibrated variability of the FTIR response for continuous 1-minute average measurements of a single tank gas over a two day period – in general the drift remained within the precision levels summarised in Table 1 over the whole period. Hammer et al. (2012) show similar stability over six days but some species show small significant drifts at the precision limit. Figure 6, also from Hammer et al. (2012, Figure 9) illustrates longer-term calibration stability with residuals of approximately daily measurements of a target tank relative to its nominal mole fractions over a 10 month period. The analyser was calibrated against 2 standards typically every day or two days. The calibration stability for all species except $\delta^{13}C$ in CO_2 meets GAW compatibility standards (Table 1). Hammer et al. (2012) conclude that for most applications weekly calibrations would be sufficient to ensure continuous WMO-GAW compatibility.

Cross sensitivities

Raw measured mole fractions of trace gases from the FTIR analyser may show small but significant residual sensitivities to pressure, temperature, flow and water vapour in the sample that are not removed by the spectrum analysis and calibration procedures. These cross-sensitivities may be due to imperfections in the measured spectra, and systematic errors in the HITRAN database, MALT analysis procedure, temperature and pressure measurements. Hammer et al. (2012) have investigated and quantified these sensitivities in detail for one analyser, and provide a set of linear correction coefficients for sensitivity to cell pressure, cell temperature, cell flow and residual water vapour amount in the spectrum. These sensitivities are typical of all analysers we have built and tested to date, and are summarised in Table 3. The uncertainty in determining water vapour cross-sensitivities is such that drying the airstream to reduce the cross-sensitivity correction is recommended for the most accurate measurements. In almost all cases, the sensitivities for reasonable variations in the quantities are small and can be corrected to within GAW compatibility targets. These corrections are applied to raw measured mole fractions before calibration to reference mole fraction scales.

Hammer et al. (2012) also found cross-sensitivity of CO and N_2O measurements to CO_2 mole fraction in the sample when analysing spectra in the region shown in Figure 3(a). This sensitivity can be significant in situations where the CO_2 mole fraction may vary by a factor of two or more between samples (for example chamber or nocturnal boundary layer measurements). However this sensitivity can be reduced to insignificance by the use of the 2097-2242 cm^{-1}

region (Figure 3(b)), which avoids most spectral interference of the absorptions of N_2O and CO with CO_2.

Calibration for $\delta^{13}C$ in CO_2

Griffith et al., (2011) and Loh et al. (2011) have considered isotopologue-specific trace gas calibration in optical analysers. Spectroscopic analysers such as the FTIR and laser analysers determine the mole fractions of isotopologues as individual species, from which the conventional δ values are directly calculated. In the following, we use IUPAC recommendations (Cohen et al., 2007; Coplen, 2008) to distinguish the following quantities:

C concentration, e.g. mol m^{-3}

χ mole fraction of trace gas e.g. μmol mol^{-1}, ppm

X isotopic abundance of an isotope or isotopologue, mol mol^{-1}

R isotope ratio

Linestrengths in the HITRAN database (Rothman et al., 2009; Rothman et al., 2005) are scaled by the natural abundance for each isotopologue, so that the actual measured isotopologue mole fraction χ_{iso} for an individual isotopologue is reported as the scaled mole fraction χ'_{iso}

$$\chi'_{iso} = \frac{\chi_{iso}}{X_{iso}} \qquad \text{Eq. (4)}$$

where X_{iso} is the natural isotopologue abundance assumed in HITRAN and shown in Table 2 for the major CO_2 isotopologues (Rothman et al., 2005). With this definition, FTIR analysis of a sample of CO_2 with all isotopes in natural abundance as specified in HITRAN and perfect calibration would report the same raw numerical value of χ'_{iso} for each isotopologue.

$\delta^{13}C$ in CO_2 is calculated from the individual mole fractions χ_{636} and χ_{626} and natural abundances X_{636} and X_{626}

$$\delta^{13}C = \frac{\chi'_{636}}{\chi'_{626}} - 1 \quad = \frac{\chi_{636}/\chi_{626}}{X_{636}/X_{626}} - 1 \qquad \text{Eq. (5)}$$

where χ_{636}/χ_{626} is here equivalent to the usual sample isotope ratio R^{13}_{sample} and X_{636}/X_{626} is equivalent to the standard isotope ratio R^{13}_{std}. $\delta^{13}C$ is normally multiplied by 1000 and expressed in ‰, but for clarity the factor 1000‰ is not explicitly written in the following. The reference

390 scale for $\delta^{13}C$ in Eq. (5) is thus that of HITRAN. Calibration of isotopologue-specific
391 measurements against reference standards calibrated to the standard Vienna Pee Dee Belomnite
392 (VPDB) corrects simultaneously for both the difference between HITRAN and VPDB scales and
393 calibration factors in the isotopologue-specific FTIR measurements of χ_{636} and χ_{626}, as detailed
394 below.

395 In applying the calibration equation (3) to individual isotopologues, we must know the individual
396 isotopologue mole fractions in the reference standards. For parent and ^{13}C isotopologues of CO_2
397 these can be calculated from the (assumed known) total CO_2 mole fractions and isotopic δ values
398 for the standard as follows:

399 The total CO_2 mole fraction is

400 $$\begin{aligned}\chi_{CO2} &= \chi_{626} + \chi_{636} + \chi_{628} + \chi_{627} + ... \\ &= \chi'_{626} X_{626} + \chi'_{636} X_{636} + \chi'_{628} X_{628} + ...\end{aligned} \quad \text{Eq. (6)}$$

401 From the definition of δ, Eq. (5)

402 $$\begin{aligned}\chi'_{636} &= (1+\delta^{13}C)\chi'_{626} \\ \chi'_{628} &= (1+\delta^{18}O)\chi'_{626} \\ \chi'_{627} &= (1+\delta^{17}O)\chi'_{626}\end{aligned} \quad \text{Eq. (7)}$$

403 and Eq. (6) can be written

404 $$\chi_{CO2} = \chi'_{626} \cdot (X_{626} + \sum_i (1+\delta^i) X_i) = \chi'_{626} \cdot X \quad \text{Eq. (8)}$$

405 where $X = X_{626} + \sum_i (1+\delta^i) X_i$ and the index *i* runs over all isotopologues except 626. Thus

406 $$\chi'_{626} = \frac{\chi_{CO2}}{X} \quad \text{Eq. (9)}$$

407 and from Eq. (7) the mole fraction of $^{13}CO_2$ is

408 $$\chi'_{636} = \frac{(1+\delta^{13}C) \cdot \chi_{CO2}}{X} \quad \text{Eq. (10)}$$

409 and similarly for the other isotopologues. To compute *X*, *all* values of δ^i and X_i must therefore
410 be known. To calculate individual isotopologue mole fractions via Eq. (10), the total CO_2 mole
411 fraction must also be known. For calibration standards $\delta^{13}C$ and $\delta^{18}O$ are usually known, and

412 with sufficient accuracy for FTIR calibrations we can assume $\delta^{17}O = 0.5 \cdot \delta^{18}O$ and all $\delta = 0$ for
413 multiply-substituted isotopologues since their contributions to the sum is very small.

414 To generate an isotopologue-specific calibration following Eq. (3) , the reference mole fractions
415 χ_{ref} should be calculated from Eqs. (9) and (10) for the regressions of χ_{meas} vs χ_{ref}. If calibrated
416 measurements of χ'_{626} and χ'_{636} are used to calculate $\delta^{13}C$ following Eq. (5), the result should
417 require no further calibration.

418 However if *uncalibrated* χ'_{626} and χ'_{636} are used to calculate $\delta^{13}C$ directly, the result is not
419 simply a linear relation to the reference δ^{13}, because in general it also depends on the mole
420 fraction of CO_2 in the sample as follows from Eq. (5):

421
$$\delta^{13}C_{meas} = \frac{\chi'_{636,meas}}{\chi'_{626,meas}} - 1 = \frac{a_{636} \cdot \chi'_{636} + b_{636}}{a_{626} \cdot \chi'_{626} + b_{626}} - 1 \qquad \text{Eq. (11)}$$

422 which can be rearranged to

423
$$\delta^{13}C_{meas} = \frac{a_{636}\chi'_{626}}{a_{626}\chi'_{626} + b_{626}} \delta^{13}C_{ref} + \frac{(a_{636} - a_{626})\chi'_{626} + b_{636} - b_{626}}{a_{626}\chi'_{626} + b_{626}} \qquad \text{Eq. (12)}$$

424 If the intercepts b are zero, Eq. (12) reduces to a simple scale shift α

425
$$\delta^{13}C_{meas} = \alpha \cdot \delta^{13}C_{ref} + (\alpha - 1) \qquad \text{Eq. (13)}$$

426 where $\alpha = \frac{a_{636}}{a_{626}}$ and the measured and reference δ scales are related by the ratio of isotopologue
427 calibration scale factors a_{636} and a_{626} only. However if b_{636} and b_{626} are non-zero the slope and
428 intercept of Eq. (12) become CO_2 mole fraction dependent and the regression over a range of
429 CO_2 mole fractions is not linear.

430 To summarise, there are thus two methods to approach $\delta^{13}C$ calibration:

431 *Method 1: Absolute calibration*

432 If a suite of reference gases of known CO_2 mole fraction and isotopic composition is available to
433 generate individual isotopologue calibrations, $\delta^{13}C$ can be calculated from Eq. (5) directly using
434 the true, calibrated values of χ'_{626} and χ'_{636} obtained following equations (9), (10) and (3). This

requires calibration of both χ'_{626} and χ'_{636} to the same level of accuracy as required for $\delta^{13}C$, typically < 0.1‰.

Method 2: Empirical calibration

If a suite of reference gases is not available, calibration for $\delta^{13}C$ can still be established from one or more calibration gases of known CO_2 mole fraction and isotopic composition, provided the CO_2 mole fraction dependence in Eq. (12) is taken into account. Eq. (12) can be rearranged in terms of the measured CO_2 mole fraction χ'_{626} as

$$\delta^{13}C_{meas} = \alpha \cdot \delta^{13}C_{ref} + (\alpha - 1) + \frac{b_{636} - \alpha \cdot (1 + \delta^{13}C_{ref}) \cdot b_{626}}{\chi'_{626,meas}}$$

$$= \alpha \cdot \delta^{13}C_{ref} + (\alpha - 1) + \frac{\beta}{\chi'_{626,meas}} \qquad \text{Eq. (14)}$$

where $\beta = b_{636} - \alpha \cdot (1 + \delta_{true}) \cdot b_{626}$ Eq. (14) reduces to Eq. (13) if the *b* values are zero.

In Eq. (14) α describes a scale shift determined by the ratio of isotopologue-specific calibration scale factors $\alpha = a_{636} / a_{626}$, while β quantifies an inverse CO_2 dependence, determined principally by the difference between b_{636} and b_{626} (since $\alpha \sim 1$ and $\delta \sim 0$). If $\delta^{13}C_{meas}$ is first corrected by subtracting the CO_2 dependence (determined empirically as described below), the scale shift α can be determined from FTIR measurements of one or more reference tanks of known $\delta^{13}C_{ref}$.

The CO_2 dependence of $\delta^{13}C_{meas}$ can be determined empirically by varying CO_2 mole fraction at constant $\delta^{13}C_{ref}$. Figure 7(a) illustrates such a case, where CO_2 is gradually stripped stepwise from a flow of sample air from a tank. The flow is split into two streams in variable portions, one of which was scrubbed completely of CO_2 with Ascarite or soda lime, and the two streams recombined. Samples taken from the recombined flow and analysed independently by Isotope Ratio Mass Spectrometry (IRMS) confirm that there was no fractionation in the stripping process. The observed dependence on CO_2 mole fraction is approximately proportional to $1/\chi_{CO2}$ as expected from Eq. (14) with a fitted value of β = -1715 ‰ ppm. However there is residual curvature in the fit to $1/\chi_{CO2}$, which can be accounted for by including a linear term $\gamma \cdot \chi_{CO2}$ in the fit. This linear term is most likely due to a very small non-linearity of the analyser response; Eq. (14) assumes that the calibration equation, Eq. (3), is linear, but a small non-linearity, represented by a quadratic term $c\chi_{ref}^2$ in Eq. (3), would lead to an additional linear term

462 $\gamma \cdot \chi'_{626}$ in Eq. (14) with the coefficient γ determined approximately by the difference between
463 c_{636} and c_{626}. The value of $c_{636} - c_{626}$ required to account for the residual curvature in Figure
464 7(a), approximately 0.005 ‰ ppm^{-1}, is small enough to be consistent with the observed residuals
465 in the individual 636 and 626 linear calibration regressions. The calibrations of Griffith et al.
466 (2011) and Hammer et al. (2012) which showed the analyser to be "linear" would not have
467 resolved a non-linearity of this magnitude.

468 With $\delta^{13}C_{meas}$ measured by FTIR corrected for the empirical CO_2 dependence as above, α can be
469 determined from Eq. (13) from measurements of one or more reference gases of known $\delta^{13}C_{ref}$.
470 Figure 7(b) shows such a case as a regression for five reference tanks, with CO_2 mole fractions
471 350-800 μmol mol^{-1} and $\delta^{13}C$ values spanning -8 to -23‰, provided by MPI for
472 Biogeochemistry, Jena. The best fit $\alpha = 1.0199$, equivalent to a scale shift of 19.9‰.

473 ## 4. Results and selected applications

474 The FTIR analyser has been used in a variety of applications for atmospheric measurements. An
475 earlier version of the analyser is described by Esler et al.(2000a, b) and some earlier applications
476 are reviewed by Griffith et al. (2002; 2000). Here we review recent applications as examples in
477 clean air monitoring, tower profile measurements and chamber flux measurements which exploit
478 the high precision and stability of the FTIR analyser.

479 ### Clean air monitoring

480 A core application of the FTIR analyser is in continuous monitoring of air at background and
481 clean air sites. From Nov 2008 – Feb 2009 we operated an analyser at the Cape Grim Baseline
482 Air Pollution Station on the NW tip of Tasmania, Australia. At Cape Grim, unpolluted southern
483 hemisphere marine air is sampled when the airflow is from the SW sector; Cape Grim is a key
484 station of the GAW and AGAGE networks. The detailed results of the 3-month comparison
485 between the FTIR analyser, LoFlo NDIR CO_2 measurements and AGAGE GC measurements for
486 CH_4, CO and N_2O have been reported previously (Griffith et al., 2011). Comparisons with LoFlo
487 and AGAGE GC measurements for the 3-month period are shown in Figure 8. (For these data
488 the CO calibration offset evident in (Griffith et al., 2011) has been corrected for non-linearity in
489 the AGAGE GC mercuric oxide reduction detector and the CO data are now in good agreement.)
490 While the LoFlo analyser clearly shows higher precision (less scatter) than the FTIR, for the
491 AGAGE GC system the FTIR is more precise for each species. Calibration biases were less than
492 the scatter in the AGAGE data.

Mobile platforms

The FTIR analyser is portable, robust and automated, and well suited to field applications. We have made FTIR measurements on eight N-S transects of the Australian continent between Adelaide (34ºS) and Darwin (12ºS) onboard the Ghan train since 2008 (Deutscher et al., 2010). For these measurements the analyser is mounted in a non-airconditioned luggage van and draws air from an inlet on the side of the train. Figure 9 illustrates results for CH_4 during the late wet season of 2008, covering 6 days in which the train travels from Adelaide in the south to Darwin in the north and return. Although the train has diesel locomotives, there is no evidence for CH_4 emissions from the engines. The observed CH_4 mole fractions are distinctly different in three regions – variable in the agricultural and more populated southern section south of 30ºS, low variability and a distinct latitudinal gradient through the arid and unpopulated centre of the continent, and large, irregular enhancements north of 23ºS affected by high seasonal monsoonal rainfall. Spikes at 23ºS, 14ºS and 12ºS coincide with long pauses at Alice Springs, Katherine and Darwin respectively where urban emissions are sampled. The enhanced CH_4 concentrations are attributed mostly to ephemeral emissions from wetlands and are being used to improve methane budgets in the Australian region (Deutscher et al., 2010; Fraser et al., 2011).

Point source emissions detection

The detection, location and quantification of leaks from potential carbon capture and storage (CCS) sites is of paramount importance for assessing the effectiveness of CCS technology for removing CO_2 from the atmosphere . In an experiment to assess the possibility of remotely detecting such a leak through atmospheric measurements, Humphries et al. (2012) combined FTIR measurements with a novel tomographic analysis to locate and quantify a point source release of CO_2 and N_2O in a flat, homogeneous landscape. Using both CO_2 and N_2O simultaneously enabled the effect of background variability on the source retrieval to be assessed, since the background of CO_2 is highly variable while that of N_2O is not. The point source was located within a 50 m circle of 8 sampling points in a bare soil paddock . The sampling points were sequentially sampled and analysed by a common FTIR analyser every 30 minutes continuously for several months, building up a catalogue of atmospheric concentrations at the 8 sampling points under a range of wind speeds and directions. A Bayesian analysis of the concentration and wind data was used to "find" the location and emission strength for each gas without detailed prior knowledge of either location or emission strength. Figure 10 shows the results of the analysis for the CO_2 release. The analysis located the position of the release within 0.7 m and the strength within 4%. Similar results were obtained for the N_2O release. The FTIR

analyser allowed the continuous autonomous operation of the sampling system for CO_2, N_2O, CH_4 and CO over several months.

Tower profile and flux measurements

Vertical profiles of trace gas concentrations measured from tall towers and flux towers probe boundary layer mixing processes and trace gas exchange between the atmosphere, surface and plant/forest communities. The Australian Ozflux tower at Tumbarumba (Leuning et al., 2005) is situated in a mature eucalypt forest in SE Australia to investigate the exchanges of energy, water and carbon in this representative biome. The Ozflux tower is 70 m high above a canopy top height of ~ 40 m. In November 2006 we operated two FTIR analysers at the Ozflux tower over a 3-week campaign, one sampling dried air for precise trace gas measurements, and one sampling undried air for stable water vapour isotope analysis. Seven inlets on the tower from 2 to 70 m above ground were sampled sequentially by both FTIR analysers each half hour to provide vertical profiles of trace gases, $\delta^{13}C$ in CO_2 and δD in water vapour every 30 min. The general intent of the campaign was to use vertical profiles of carbon and water isotope compositions to partition water vapour between evaporation and transpiration, and CO_2 between photosynthetic uptake and release by respiration. The campaign set up and water vapour isotope analysis has been described in detail elsewhere (Haverd et al., 2011). Time series of trace gases and $\delta^{13}C$ are shown in Figure 11. For CO_2 and $\delta^{13}C$ in CO_2 (Figure 11a) strong vertical gradients are observed in the canopy at night when canopy turbulence is low, but above the canopy the air is generally better mixed and gradients are much smaller. There is strong anti-correlation between CO_2 and $\delta^{13}C$ because the added respired CO_2 is depleted in ^{13}C. Keeling plots such as shown in Figure 12 show intercepts around -27‰, consistent with respiration from the predominantly C3 plants that dominate this forest. However during daytime, when canopy turbulence and boundary layer mixing is stronger, the air is well mixed in and above the canopy and vertical gradients are smoothed out, making the determination of partitioning from isotopic profiles during daytime impractical. Figure 11(b) shows similar data for CH_4 and N_2O, indicating clear uptake of CH_4 at the surface (decreasing mole fractions near the ground), and barely detectable N_2O emission (increasing mole fractions near the ground).

Vertical gradients of trace gas concentrations can be used to calculate surface exchange fluxes if the turbulent diffusion can be quantified (e.g. Monteith and Unsworth, 1990). This technique was not practical in the forest environment, where turbulence within the canopy was high during the day and concentration gradients were small, or gradients were high at night but turbulence

was suppressed. Flux gradient measurements are suited to agricultural environments above a uniform surface such as grass or crop. Here the high precision of the FTIR analyser is well suited to measurement of the small concentration gradients that exist. An early application to agricultural flux gradient measurements was able to quantify CO_2 fluxes, but was not sufficiently precise for background N_2O or CH_4 fluxes except following rain when N_2O emissions are enhanced (Griffith et al., 2002). Based on the Fick's Law relationship between flux and concentration gradient

$F = K(z)\frac{\partial C}{\partial z}$, F = flux, K = diffusion constant, z = height and C = concentration,

the measurement precisions described in Table 1, a typical turbulent diffusion constant of 0.1 – 0.2 $m^2\ s^{-1}$, and a vertical scale for measuring gradients of the order of 1 m, Table 4 provides estimates of minimum detectable fluxes for the FTIR analyser using the flux gradient technique. Eddy accumulation methods such as Relaxed Eddy Accumulation (REA) or Disjunct Eddy Accumulation (DEA) allow more measurement time to achieve higher trace gas measurement precision, and hence improved flux detection limits. We have applied the FTIR analyser in both REA and DEA techniques, which will be reported in forthcoming publications.

Chamber measurements

Micrometeorological flux measurement techniques are usually not able to resolve background fluxes of methane, nitrous oxide and trace gases other than CO_2 because the small vertical gradients cannot be resolved with sufficient speed or precision by existing measurement techniques. In many cases, chamber measurements offer the only feasible method to estimate small fluxes, despite their limitations (eg. site inhomogeneity and disturbance, microclimate perturbation) (Livingstone and Hutchinson, 1995). The FTIR analyser coupled to automated surface flux chambers provides a useful technique for greenhouse gas exchange measurements at the earth's surface with several advantages:

- Simultaneous measurement of greenhouse gases CO_2, CH_4 and N_2O, as well as CO and $\delta^{13}C$ in CO_2
- High precision enabling the measurement of small fluxes
- Continuous measurements with 1 minute averaging time or better, allowing assessment of the linearity of concentration changes and hence chamber leakage or other secondary processes occurring in the chamber

- Continuous fully automated operation
- The isotopic specificity of FTIR analysis allows the option to include isotopic labelling to elucidate the mechanisms of trace gas emissions.

We have carried out several FTIR-chamber flux studies in a variety of agricultural and natural settings. A fully automated system has operated continuously since 2004 measuring N_2O fluxes from irrigated and non-irrigated pasture in Victoria, Australia (Kelly et al., 2008), and another system was deployed over a complete sugar cane growth cycle in northern Australia (Denmead et al., 2010). Both studies were based on earlier FTIR systems but provided continuous measurements over periods of months to years.

Here we briefly describe two current examples of chamber flux measurements with the FTIR analyser described here – full details will be published elsewhere. The Quasom field experiment at the Max Planck Institute for Biogeochemistry in Jena, Germany, (https://www.bgc-jena.mpg.de/bgp/index.php/Main/QuasomFieldExperiment) investigates the cycling of carbon through an entire growing cycle of an annual crop by measurements of all carbon pools and fluxes, including isotopic ^{13}C labelling and discrimination measurements. The FTIR analyser is coupled to 12 soil flux chambers in the field experiment and sequentially samples air from the chambers as each goes through a closure cycle. The sampled air is recirculated back to the chambers. The system has operated continuously since June 2011, with a 1-minute measurement-averaging time and typically ninety 15-minute chamber closures per day. The $^{13}CO_2$ isotopic measurements were calibrated using the procedures described in section 3, based on measurements of whole air reference gases provided by MPI-BGC. Results agree well for both absolute and empirical calibration methods, with 1σ precision of better than 0.1‰.

Figure 13 illustrates trace gas measurements from a sequence of closures of seven individual chambers, made in the evening when there is no photosynthetic CO_2 uptake. Individual chambers show considerable variability, but all are sources for CO_2 and N_2O, sinks for CO, and show complex behaviour for CH_4. CO_2 emissions correlate with decreasing $\delta^{13}C$ because the respired CO_2 is depleted in ^{13}C. Figure 14 shows a typical night-time Keeling plot of $\delta^{13}C$ vs 1/(CO_2 mole fraction) from a single chamber closure. The $\delta^{13}C$ signature of the respired CO_2 in the chamber is equal to the y-intercept of the plots, -31.8 and -32.1‰ for the empirical and absolute calibrations respectively.

The second example of chamber flux measurements includes novel measurements of N_2O isotopologues in the field (Phillips et al., 2012). Fluxes of $^{14}N^{14}NO$, $^{14}N^{15}NO$, $^{15}N^{14}NO$ and

$^{15}N^{15}NO$ were measured pre- and post-addition of ^{15}N labelled substrate (potassium nitrate or urea) to the soil at a pasture site with a pneumatically-controlled, automated chamber system. Chambers were controlled and sampled sequentially by the FTIR analyser for 30 minutes each, with analysed air recirculated back to the chamber in a closed loop. Each chamber closed for 18 minutes out of the 30 minute cycle and spectra were measured continuously with 1-minute averaging time. Isotopologue amounts were determined by analysis of a spectral window near 2200 cm^{-1} in the strong ν_3 band of N_2O. A total of 40 flux measurements (chamber closures) were collected each day from the five chambers between 1 Dec 2011 and 30 Jan 2012. Four chambers received ^{15}N in solution and one chamber received water only. Only $^{14}N^{14}NO$ was detected for the water-only chamber, ^{15}N isotopologues in natural abundance were below quantification limits. All four isotopologues were quantified with better than 1 nmol mol^{-1} precision for the four chambers dosed with ^{15}N. Figure 15 shows the instantaneous and cumulative fluxes of all N_2O isotopologues from 4 days before ^{15}N addition to 8 days after. ^{15}N-labelled N_2O emissions decreased to near-zero levels after 8 days, while emissions of unlabelled N_2O continued from the unlabelled soil nitrogen pool. This experiment enabled the measurement of additional N_2O emitted due to fertiliser addition independent of the background N_2O emission flux. Approximately 1– 2% of the added N was emitted as N_2O.

5. Conclusions

The FTIR trace gas analyser provides simultaneous, continuous, high precision analysis of the atmospheric trace gases CO_2, CH_4 and N_2O and CO in air. A 1-5 minute averaging time is sufficient to achieve repeatability meeting GAW measurement compatibility targets for clean air measurements, and with careful calibration the accuracy is of similar magnitude (Hammer et al., 2012). In addition, parallel measurements of $\delta^{13}C$ in CO_2 from the same air samples with precision only slightly less than GAW targets are obtained. The analyser is suited to a wide range of applications in atmospheric trace gas measurements, including composition monitoring at clean air baseline stations and on mobile platforms, micrometeorological and chamber flux measurements, and isotopic measurements of atmospheric trace gases.

6. Acknowledgements

We gratefully acknowledge the contributions, comments and feedback from many colleagues over the years of development and application of the FTIR analyser. These include Dan Smale, Vanessa Sherlock, Thorsten Warneke, Katinka Petersen for feedback on the instrument operation and performance, Grant Kassell and other staff of Ecotech Pty Ltd for developments in the

652 commercialisation of the analyser, many staff of CSIRO and the Cape Grim Baseline Air
653 Pollution Station for measurements at Cape Grim, GASLAB and the Ozflux tower site, Marion
654 Schrumpf and Armin Jordan for measurements at the Quasom site in Jena, and Rebecca Phillips
655 for collaboration in the N_2O isotope chamber studies.

656

657

References

Allan, D.: Statistics of atomic frequency standards, Proc. IEEE, 54, 221-230, 1966.

Anderson, R. J., and Griffiths, P. R.: Errors in absorbance measurements in infrared Fourier transform spectrometry because of limited instrument resolution, Analytical Chemistry, 47, 2339-2347, 1975.

Cohen, E. R., Cvitas, T., Frey, J. G., Holmstroem, B., Kuchitsu, K., Marquardt, R., Mills, I., Pavese, F., Quack, M., Stohner, J., Strauss, H. L., Takami, M., and Thor, A. J.: Quantities, Units and Symbols in Physical Chemistry, IUPAC, RSC Publishing, Cambridge, 2007.

Coplen, T. B.: Explanatory glossary of terms used in expression of relative isotope ratios and gas ratios, IUPAC, 27. Available at http://old.iupac.org/reports/provisional/abstract08/coplen_prs.pdf, 2008.

Davis, S. P., Abrams, M. C., and Brault, J. W.: Fourier Transform Spectrometry, Academic Press, 2001.

Denmead, O. T., Macdonald, B. C. T., Bryant, G., Naylor, T., Wilson, S., Griffith, D. W. T., Wang, W. J., Salter, B., White, I., and Moody, P. W.: Emissions of methane and nitrous oxide from Australian sugarcane soils, Agric. For. Meteorol., 150, 748-756, 10.1016/j.agrformet.2009.06.018, 2010.

Deutscher, N. M., Griffith, D. W. T., Paton-Walsh, C., and Borah, R.: Train-borne measurements of tropical methane enhancements from ephemeral wetlands in Australia., J. Geophys. Res., 115, D15304, doi:15310.11029/12009JD013151., 2010.

Esler, M. B., Griffith, D. W. T., Wilson, S. R., and Steele, L. P.: Precision trace gas analysis by FT-IR spectroscopy 1. Simultaneous analysis of CO_2, CH_4, N_2O and CO in air, Analytical Chemistry, 72, 206-215, 2000a.

Esler, M. B., Griffith, D. W. T., Wilson, S. R., and Steele, L. P.: Precision trace gas analysis by FT-IR spectroscopy 2. The $^{13}C/^{12}C$ isotope ratio of CO_2, Analytical Chemistry, 72, 216-221, 2000b.

Francey, R. J., Trudinger, C. M., Schoot, M. v. d., Krummel, P. B., Steele, L. P., and Langenfelds, R. L.: Differences between trends in atmospheric CO_2 and the reported trends in anthropogenic CO_2 emissions, Tellus, 62B, 316-328, 10.1111/j.1600-0889.2010.00472.x, 2010.

Fraser, A., Miller, C. C., Palmer, P. I., Deutscher, N. M., Jones, N. B., and Griffith, D. W. T.: The Australian methane budget: New insights from surface and train-borne measurements, J. Geophys. Res., 116, http://dx.doi.org/10.1029/2011JD015964, 2011.

GAW: Report no. 194. 15th WMO/IAEA Meeting of Experts on Carbon Dioxide, Other Greenhouse Gases and Related Tracers Measurement Techniques, GenevaWMO/TD-No. 1553, 2011.

Griffith, D., Deutscher, N., Krummel, P., Fraser, P., Steele, P., Schoot, M. v. d., and Allison, C.: The UoW FTIR trace gas analyser: comparison with LoFlo, AGAGE and tank measurements at

CApe Grim and GASLAB, in: Baseline Atmospheric Program (Australia) 2007-2008, edited by: Derek, P. K. a. N., CSIRO, Melbourne, http://www.bom.gov.au/inside/cgbaps/baseline.shtml, 2011.

Griffith, D. W. T.: Synthetic calibration and quantitative analysis of gas phase infrared spectra, Appl. Spectrosc., 50, 59-70, 1996.

Griffith, D. W. T., and Jamie, I. M.: FTIR spectrometry in atmospheric and trace gas analysis, in: Encyclopedia of Analytical Chemistry, edited by: Meyers, R. A., Wiley, 1979-2007, 2000.

Griffith, D. W. T.: FTIR measurements of atmospheric trace gases and their fluxes, in: Handbook of vibrational spectroscopy, edited by: Chalmers, J. M., and Griffiths, P. R., John Wiley & Sons, 2823-2841, 2002.

Griffith, D. W. T., Leuning, R., Denmead, O. T., and Jamie, I. M.: Air-Land Exchanges of CO_2, CH_4 and N_2O measured by FTIR Spectroscopy and Micrometeorological Techniques, Atmos. Environ., 38, 1833-1842, 2002.

Griffith, D. W. T.: Non linear least squares retrieval of trace gas concetrations from FTIR spectra, Appl. Spectrosc., in prep., 2012.

Griffiths, P. R., and de Haseth, J. A.: Fourier Transform Infrared Spectrometry, 2nd Edition, Wiley, 2007.

Haaland, D. M.: Methods to include Beer's Law non-linearities in quantitative spectral analysis, in: Computerised Quantitative Infrared Analysis, ASTM-STP-934, edited by: McClure, G. L., American Society for Testing and Materials, Philadelphia, 78-94, 1987.

Hammer, S., Griffith, D. W. T., Konrad, G., Verdag, S., Caldow, C., and Levin, I.: Assessment of a multi-species in situ FTIR for precise atmospheric greenhouse gas observations, Atmospheric Measurement Techniques (Discussions), This issue, 2012.

Haverd, V., Cuntz, M., Griffith, D., Keitel, C., Tadros, C., and Twining, J.: Measured deuterium in water vapour concentration does not improve the constraint on the partitioning of evapotranspiration in a tall forest canopy, as estimated using a soil vegetation atmosphere transfer model, Agric. For. Meteorol., 151, 645-654, 2011.

Hofmann, D. J., Butler, J. H., Dlugokencky, E. J., Elkins, J. W., Masarie, K., Montzka, S. A., and Tans, P.: The role of carbon dioxide in climate forcing from 1979 to 2004: Introduction to the Annual Greenhouse Gas Index, Tellus, 58B, 614-619, 2006.

Humphries, R., Jenkins, C., Leuning, R., Zegelin, S., Griffith, D., Caldow, C., Berko, H., and Feitz, A.: Atmospheric Tomography: A Bayesian Inversion Technique for Determining the Rate and Location of Fugitive Emissions, Environ. Sci. Technol., 46, 1739-1746, dx.doi.org/10.1021/es202807s, 2012.

IPCC: Contribution of Working Group I to the Fourth Assessment Report of the Intergovernmental Panel on Climate Change, Geneva, 2007.

JCGM: Evaluation of measurement data — Guide to the expression of uncertainty in measurement (GUM), Joint Committee for Guides in Measurement - Working Group 1 (JCGM/WG1JCGM 100:2008, 2008.

734 Johnson, T. J., Profeta, L. T. M., Sams, R. L., Griffith, D. W. T., and L.Yokelson, R.: An
735 Infrared Spectral Database for Detection of Gases Emitted by Biomass Burning, Vibrational
736 Spectroscopy, 53, 97-102, doi:10.1016/j.vibspec.2010.02.010, 2010.

737 Keeling, C. D., Whorf, T. P., Wahlen, M., and Plicht, J. v. d.: Interannual extremes in the rate of
738 rise of atmospheric carbon dioxide since 1980, Nature, 375, 666-670, 1995.

739 Kelly, K. B., Phillips, F. A., and Baigent, R.: Impact of dicyandiamide application on nitrous
740 oxide emissions from urine patches in northern Victoria, Australia., Australian Journal of
741 Experimental Agriculture, 48, 156-159, doi: 10.1071/EA07251, 2008.

742 Langenfelds, R., Steele, P., Leist, M., Krummel, P. B., Spencer, D., and Howden, R.:
743 Atmospheric methane, carbon dioxide, hydrogen, carbon monoxide, and nitrous oxide from Cape
744 Grim flask air samples analysed by gas chromatography, in: Baseline Atmospheric Program
745 (Australia) 2007-2008, edited by: Derek, N., and Krummel, P. B., Bureau of Meteorology and
746 CSIRO Marine and Atmospheric Research, Melbourne, 62-66,
747 http://www.bom.gov.au/inside/cgbaps/baseline.shtml, 2011.

748 Leuning, R., Cleugh, H. A., Zegelin, S. J., and Hughes, D.: Carbon and water fluxes over a
749 temperate *Eucalyptus* forest and tropical wet/dry savanna in Australia: measurements and
750 comparison with MODIS remote sensing estimates, Agric. For. Meteorol., 129, 2005.

751 Livingstone, G. P., and Hutchinson, G. L.: Enclosure-based measurements of trace gas exchange:
752 applications and sources of error, in: Biogenic Trace Gases: Measuring emissions from soil and
753 water, edited by: Matson, P. A., and Harriss, R. C., Blackwell Science, 1995.

754 Loh, Z. M., Steele, L. P., Krummel, P. B., Schoot, M. v. d., Etheridge, D. M., Spencer, D. A.,
755 and Francey, R. J.: Linking Isotopologue Specific Measurements of CO2 to the Existing
756 International Mole Fraction Scale, 15th WMO/IAEA Meeting of Experts on Carbon Dioxide,
757 Other Greenhouse Gases and Related Tracers Measurement Techniques (WMO/GAW report no.
758 194), Jena, Germany, August 2009, 2011,

759 Monteith, J. L., and Unsworth, M. H.: Principles of Environmental Physics, Edward Arnold,
760 London, 1990.

761 Parkes, S. D., Element, A., Griffith, D. W. T., Haverd, V., and Wilson, S. R.: An in-situ FTIR
762 analyser for simultaneous real-time water vapour stable isotope and greenhouse gas
763 measurements, Atmospheric Measurement Techniques, in preparation, 2012.

764 Phillips, R., Griffith, D. W. T., Dijkstra, F., Lugg, G., Lawrie, R., and Macdonald, B.:
765 Continuous field measurement of N_2O isotopologues using FTIR spectroscopy following ^{15}N
766 addition, American Geophysical Union Fall meeting, San Francisco, 2012,

767 Popa, M. E., Gloor, M., Manning, A. C., Jordan, A., Schultz, U., Haensel, F., Seifert, T., and
768 Heimann, M.: Measurements of greenhouse gases and related tracers at Bialystok tall tower
769 station in Poland, Atmos. Meas. Tech., 3, 407-427, 2010.

770 Press, W. H., Teukolsky, S. A., Vetterling, W. T., and Flannery, B. P.: Numerical Recipes,
771 Cambridge University press, 1992.

772 Prinn, R. G., Weiss, R. F., Fraser, P. J., Simmonds, P. G., Cunnold, D. M., Alyea, F. N.,
773 O'Doherty, S., Salameh, P., Miller, B. R., Huang, J., Wang, R. H. J., D.E.Hartley, Harth, C.,

774 Steele, L. P., Sturrock, G., Midgley, P. M., and McCulloch, A.: A history of chemically and
775 radiatively important gases in air deduced from ALE/GAGE/AGAGE, J. Geophys. Res., 105,
776 17751-17792, 2000.

777 Ravishankara, A. R., Daniel, J. S., and Portmann, R. W.: Nitrous oxide (N_2O): the dominant
778 ozone-depleting substance emitted in the 21st century, Science, 326, 123-125, 2009.

779 Rothman, L. S., Jacquemart, D., Barbe, A., Benner, D. C., Birk, M., Brown, L. R., Carleer, M.
780 R., C. Chackerian, J., Chance, K., Dana, V., Devi, V. M., Flaud, J.-M., Gamache, R. R.,
781 Goldman, A., Hartmann, J.-M., Jucks, K. W., Maki, A. G., Mandin, J.-Y., Massie, S. T., Orphali,
782 J., Perrin, A., Rinsland, C. P., Smith, M. A. H., Tennyson, J., Tolchenov, R. N., Toth, R. A.,
783 Auwera, J. V., Varanasi, P., and Wagner, G.: The HITRAN 2004 molecular spectroscopic
784 database, Journal of Quantitative Spectroscopy & Radiative Transfer, 96, 139-204, 2005.

785 Rothman, L. S., Gordon, I. E., Barbe, A., Benner, D. C., Bernath, P. E., Birk, M., Boudon, V.,
786 Brown, L. R., Campargue, A., Champion, J. P., Chance, K., Coudert, L. H., Dana, V., Devi, V.
787 M., Fally, S., Flaud, J. M., Gamache, R. R., Goldman, A., Jacquemart, D., Kleiner, I., Lacome,
788 N., Lafferty, W. J., Mandin, J. Y., Massie, S. T., Mikhailenko, S. N., Miller, C. E., Moazzen-
789 Ahmadi, N., Naumenko, O. V., Nikitin, A. V., Orphal, J., Perevalov, V. I., Perrin, A., Predoi-
790 Cross, A., Rinsland, C. P., Rotger, M., Simeckova, M., Smith, M. A. H., Sung, K., Tashkun, S.
791 A., Tennyson, J., Toth, R. A., Vandaele, A. C., and Vander Auwera, J.: The HITRAN 2008
792 molecular spectroscopic database, Journal of Quantitative Spectroscopy & Radiative Transfer,
793 110, 533-572, 2009.

794 Sharpe, S. W., Johnson, T. J., Sams, R. L., Chu, P. M., Rhoderick, G. C., and Johnson, P. A.:
795 Gas phase databases for quantitative infrared spectroscopy, Appl. Spectrosc., 58, 1452-1461,
796 2004.

797 Smith, T. E. L., Wooster, M. J., Tattaris, M., and Griffith, D. W. T.: Absolute accuracy
798 evaluation and sensitivity analysis of OP-FTIR NLS retrievals of CO_2, CH_4 and CO over
799 concentrations ranging from those of ambient atmospheres to highly polluted plumes.,
800 Atmospheric Measurement Techniques, 4, 97-116, 2011.

801 Steele, L. P., Krummel, P., D, S., Rickard, C., Baly, S., Langenfelds, R., and Schoot, M. v. d.:
802 Baseline carbon dioxide monitoring, in: Baseline Atmospheric Program (Australia) 2007-2008,
803 edited by: Derek, N., and Krummel, P., Bureau of Meteorology and CSIRO Marine and
804 Atmospheric Research, Melbourne, 51-53, http://www.bom.gov.au/inside/cgbaps/baseline.shtml,
805 2011.

806 Tuzson, B., Henne, S., Brunner, D., Steinbacher, M., Mohn, J., Buchmann, B., and Emmenegger,
807 L.: Continuous isotopic composition measurements of tropospheric CO2 at Jungfraujoch (3580
808 m a.s.l.), Switzerland: real-time observation of regional pollution events, Atmos. Chem. Phys.,
809 11, 1685-1696, 10.5194/acp-11-1685-2011, 2011.

810 van der Laan, S., Neubert, R. E. M., and Meier, H. A. J.: A single gas chromatograph for
811 accurate atmospheric mixing ratio measurements of CO_2, CH_4, N_2O, SF_6 and CO, Atmospheric
812 Measurement Techniques, 2, 549-559, 2009.

813 Vermeulen, A. T., Hensen, A., Popa, M. E., van den Bulk, W. C. M., and Jongejan, P. A. C.:
814 Greenhouse gas observations from Cabauw Tall Tower (1992–2010), Atmos. Meas. Tech., 4,
815 617-644, 10.5194/amt-4-617-2011, 2011.

816 Werle, P., Muecke, R., and Slemr, F.: The limits of signal averaging in trace gas monitoring by
817 tunable diode laser absorption spectroscopy (TDLAS), Appl. Phys., B57, 131-139, 1993.

818

819

Tables

Table 1. Global mean mole fractions, GAW measurement compatibility requirements, and FTIR analyser measurement precision (Allan deviation for 1- and 10-min averaging times) for target trace gases.

Species	Approximate global mean mole fraction, 2010 (GAW, 2011)	GAW recommended compatibility target	FTIR measurement repeatability	
			1 min	10 min
CO_2 / μmol mol^{-1}	389	0.1 (NH) 0.05 (SH)	0.02	0.01
CH_4 / nmol mol^{-1}	1808	2	0.2	0.06
N_2O / nmol mol^{-1}	323	0.1	0.1	0.03
CO / nmol mol^{-1}	100 (NH) 50 (SH)	2	0.2	0.08
$\delta^{13}C$-CO_2 / ‰	-8.2	0.01	0.07	0.02

827 **Table 2. HITRAN isotopologue natural abundances**

Isotopologue	Notation	Abundance X_{iso}
$^{16}O^{12}C^{16}O$	626	0.98420
$^{16}O^{13}C^{16}O$	636	0.01106
$^{16}O^{12}C^{18}O$	628	0.0039471
$^{16}O^{12}C^{17}O$	627	0.000734

828

829

Table 3. Linear sensitivities dχ/d(quantity) of trace gas measurements to quantities pressure, temperature, flow and other trace gases in the sample. From (Hammer et al., 2012).

*** CO_2 sensitivity is more accurately treated as proportional to inverse mole fraction as described above.**

$\frac{d\chi}{d(quantity)}$	**CO_2 μmol mol^{-1}**	**$\delta^{13}C$ - CO_2 ‰**	**CH_4 nmol mol^{-1}**	**CO nmol mol^{-1}**	**N_2O nmol mol^{-1}**
Pressure hPa	0.0085	0.005	0.031	0.006	0.007
Equil. Temp. ºC	<0.8	0.6	<1.6	<1	0.6
Disequil. Temp. ºC	2.07	4.1	-4.6	10.2	3.2
Flow L min^{-1}	0.15	-0.9	<4	<2	< -0.8
Residual H_2O μmol mol^{-1}	.04	-	<0.2	<0.2	-
CO_2 μmol mol^{-1}	-	0.006*	-	0.006	0.008

836 **Table 4. Approximate minimum detectable fluxes achievable with the FTIR analyser using the flux gradient**
837 **technique under typical turbulent diffusion conditions: diffusion coefficient 0.1-0.2 $m^2 s^{-1}$, vertical gradient**
838 **scale ~ 1 m.**

	Gradient measurement precision	Minimum detectable flux
CO_2	0.1 μmol mol^{-1}	0.04 $mgCO_2$ m^{-2} s^{-1}
N_2O	0.1 nmol mol^{-1}	20 ngN m^{-2} s^{-1}
CH_4	0.2 nmol mol^{-1}	30 ng CH_4 m^{-2} s^{-1}

839

840

Figure captions

Figure 1. The mid-infrared absorption spectrum of clean air in a 24 m cell. Red: undried air, blue: dried air. Positions of main absorption bands of target gases CO_2, CH_4, CO and N_2O are shown. More detail of individual regions is shown in Figure 3.

Figure 2. Schematic view of the sampling gas manifold. For valve functions see text.

Figure 3. Typical non-linear least squares fits to a spectrum of dry air in four spectral regions. (a) 2150-2310 cm^{-1}, fitting CO_2 isotopologues, CO, N_2O and H_2O; (b) 2097 – 2242 cm^{-1}, optimised for N_2O and CO, also fitting CO_2; (c) 3001 – 3150 cm^{-1}, fitting CH_4 and H_2O; (d) 3520-3775 cm^{-1}, fitting CO_2 and H_2O. Contributions from individual species are shown in colours, offset +0.2 units for clarity.

Figure 4. Time series (upper panels) and Allan deviation (lower panels) plots of consecutive 1-minute average measurements of CO_2, CH_4, CO, N_2O and $\delta^{13}C$ in CO_2 for an unchanging air sample in the FTIR analyser. The dashed lines have a slope of -0.5 (log-log) and show the expected behaviour of the Allan deviation vs time for random (white) noise.

Figure 5. Residuals with 1σ error bars from linear regressions of raw FTIR measured mole fractions against reference mole fractions for a suite of tanks maintained by the University of Heidelberg. (Data and further details from Hammer et al. (2012))

Figure 6. Measurement residuals with 1σ error bars relative to a reference value for a single target tank over a 10 month period (from Hammer et al., 2012). During this period, the FTIR analyser was based in Heidelberg except for two field campaigns at Cabauw, Netherlands (CBW) and Houdelaincourt, France (OPE). "Ecotech" refers to a rebuild of the instrument to include the mass flow controller (section 2) and "EPC" refers to the addition of an electronic pressure controller upstream of the analyser in the sample airstream. "No evac" refers to a period where ambient and target gas in the cell was exchanged by switching flow alone, without evacuation of the cell.

Figure 7. (a) Empirical dependence of raw measured $\delta^{13}C$ in CO_2 on the inverse CO_2 mole fraction, $1/\chi_{CO2}$, following Eq. (14). Each point is from a 1 minute average spectrum measured during the stepwise stripping sequence from 800 to 330 μmol mol^{-1} CO_2. (b) Fit of Eq. (13) to $\delta^{13}C$ measured by FTIR and corrected for

CO_2 dependence (see text) against reference values for five reference tanks with CO_2 mole fractions 350-800 μmol mol^{-1} and $\delta^{13}C$ values -8 to -23‰. Each point is from a 1-minute average spectrum after filling the measurement cell with reference gas. From the fit α = 1.0199, equivalent to a scale shift of 19.9‰.

Figure 8. Comparisons of FTIR measurements over a 3-month campaign at Cape Grim with LoFlo (CO_2) and AGAGE (CH_4, CO, N_2O) GC measurements. Red: LoFlo/AGAGE. Blue: FTIR. Upper panels: time-coincident measurements. Lower panels: difference. Full circles represent baseline air periods, open circles non-baseline conditions. From (Griffith et al., 2011) with updates to AGAGE CO data calibration (see text for details).

Figure 9. Measurements of CH_4 along a N-S transect aboard the Ghan train from Adelaide (34ºS) to Darwin (12ºS), March-April 2008. Figure adapted from (Deutscher et al., 2010), see text for summary.

Figure 10. Result of the FTIR-tomography detection of a CO_2 point source release in a 50 x 50 m area. In the left hand frame x marks the actual point location (0, 0 m) from where CO_2 and N_2O were released, and 1-8 mark the locations of the sampling points for the FTIR analyser. The contours plot the a posteriori probability for the source point location determined from the atmospheric measurements (-0.5, 0.5 m). The right hand plot shows the known release rate (56.7 ± 0.8 g min^{-1}) and the a posterior probability determined from the measurements (54.9 ± 4 (1σ) g min^{-1}). Figure from Humphries et al. (2012), Figure 5.

Figure 11. Time series of trace gas mole fractions and $\delta^{13}C$ in CO_2 during a 3-week campaign at the Ozflux tower site near Tumbarumba, SE Australia in Nov 2006. Seven-point vertical profiles of each species from 2 – 70 m were measured every 30 minutes; colours represent measurements at heights above the surface shown in the legend. The top of the forest canopy is approx 40m above the surface.

Figure 12. Keeling plot of $\delta^{13}C$ vs 1/[CO_2] for two nights drawn from the data shown in Figure 11. The mean intercept is -26.8‰, indicative of respiration from the dominant C3 plants in the forest.

Figure 13. Time sequence of mole fractions of CO_2, CH_4, N_2O, CO and $\delta^{13}C$ in CO_2 measurements from seven sequential chamber closures in the Quasom experiment, 1 July 2011. See text for details.

Figure 14. Keeling plot of $\delta^{13}C$ vs 1/χ_{CO2} for a typical single chamber closure from the data of Figure 13. The two plots are derived from the absolute and empirical $\delta^{13}C$ calibration methods described in section 3.

907

908

909 **Figure 15. N_2O isotopologue emissions from pasture before and after addition of ^{15}N as nitrate to the soil on**
910 **17 Dec 2011. Approximately 25mm of rainfall fell on 20-21 Dec 2011. See text for further detail.**

911

912

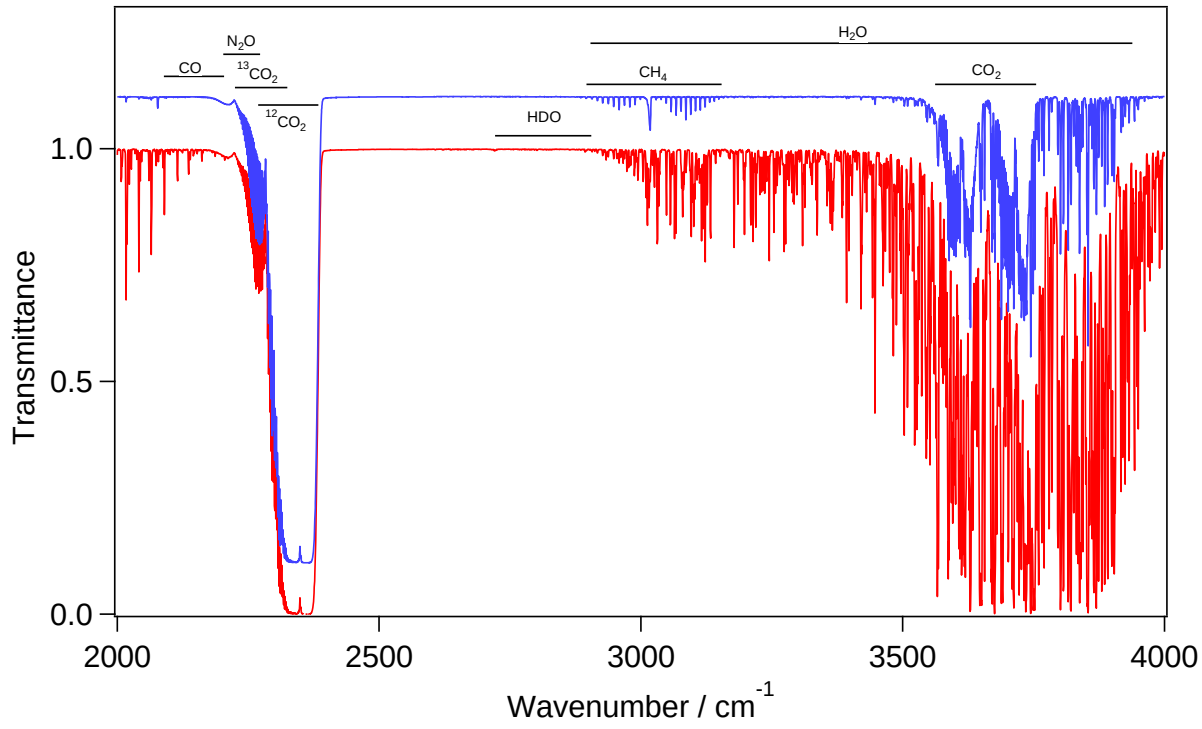

913

914 Figure 1. The mid-infrared absorption spectrum of clean air in a 24 m cell. Red: undried air,
915 blue: dried air. Positions of main absorption bands of target gases CO2, CH4, CO and N2O are
916 shown. More detail of individual regions is shown in Figure 3.

917

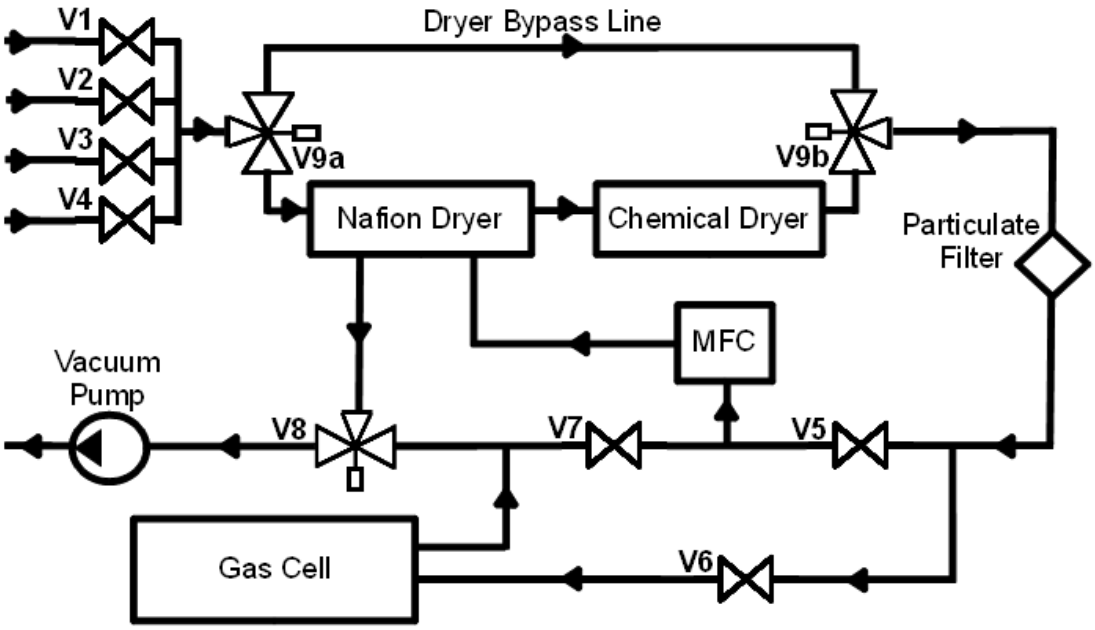

Figure 2. Schematic view of the sampling gas manifold. For valve functions see text.

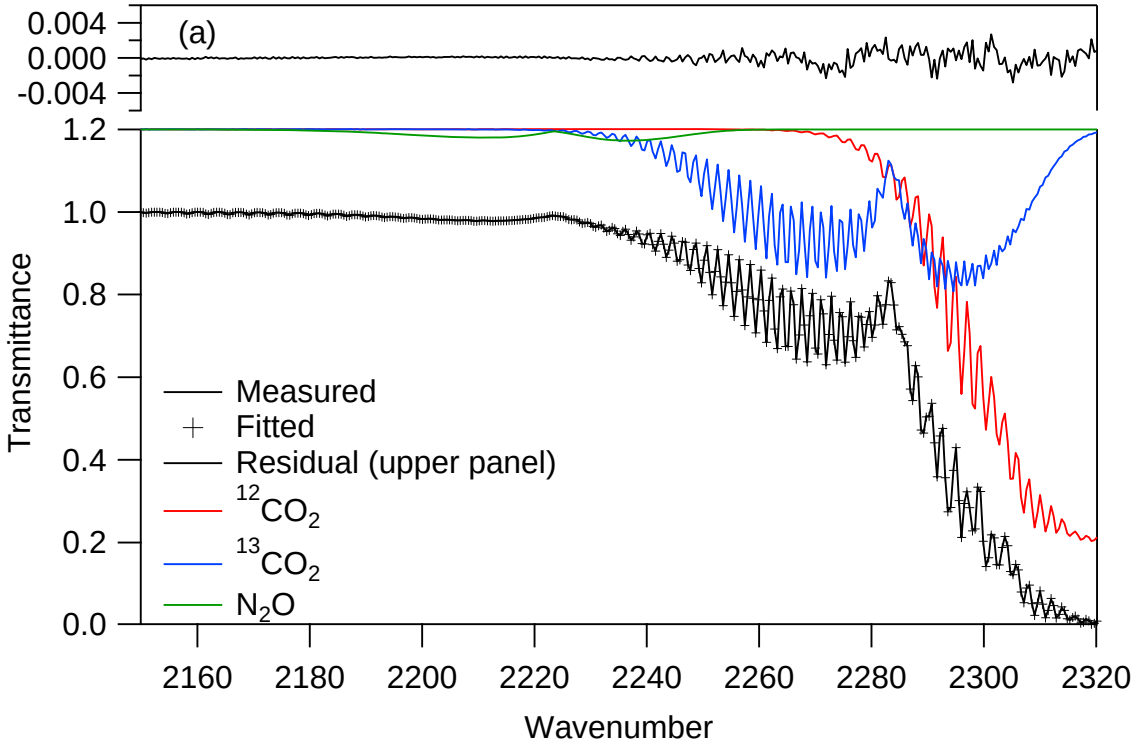
(a)
0.004
0.000
-0.004
1.2
1.0
0.8
0.6
0.4
0.2
0.0
Transmittance
Measured
Fitted
Residual (upper panel)
12CO2
13CO2
N2O
2160
2180
2200
2220
2240
2260
2280
2300
2320
Wavenumber

921

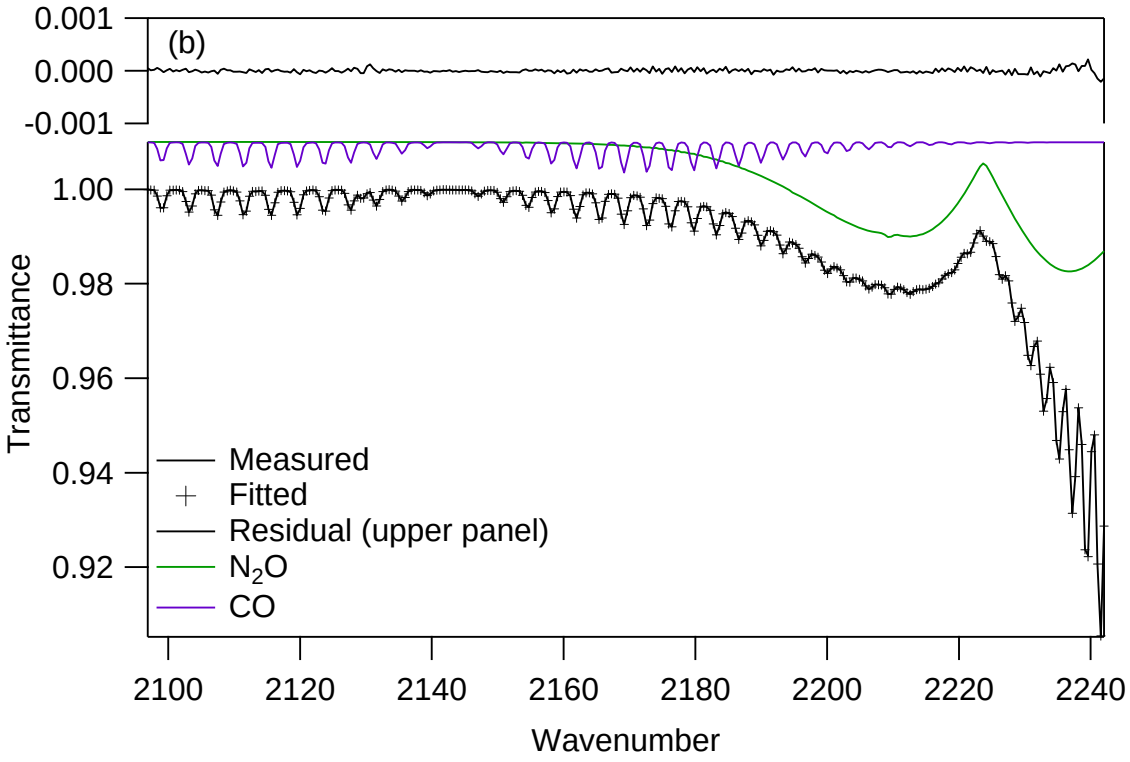
(b)
0.001
0.000
-0.001
1.00
0.98
0.96
0.94
0.92
Transmittance
Measured
Fitted
Residual (upper panel)
N2O
CO
2100
2120
2140
2160
2180
2200
2220
2240
Wavenumber

922

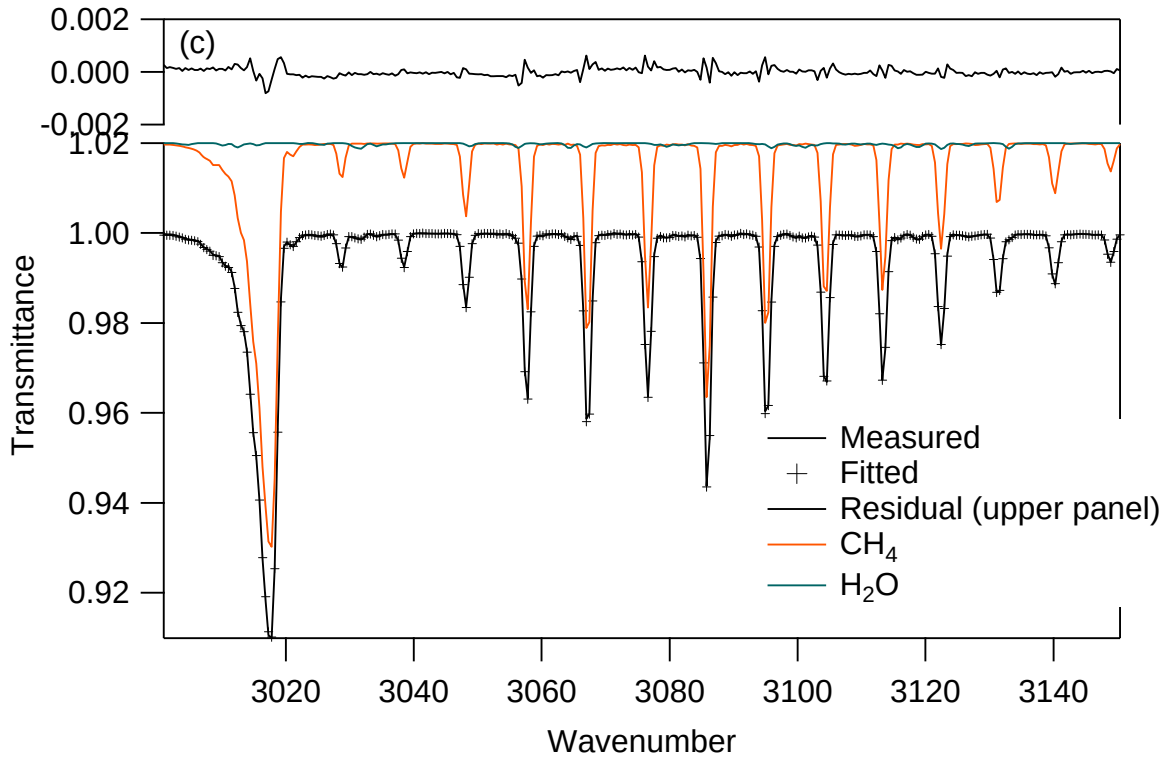

923

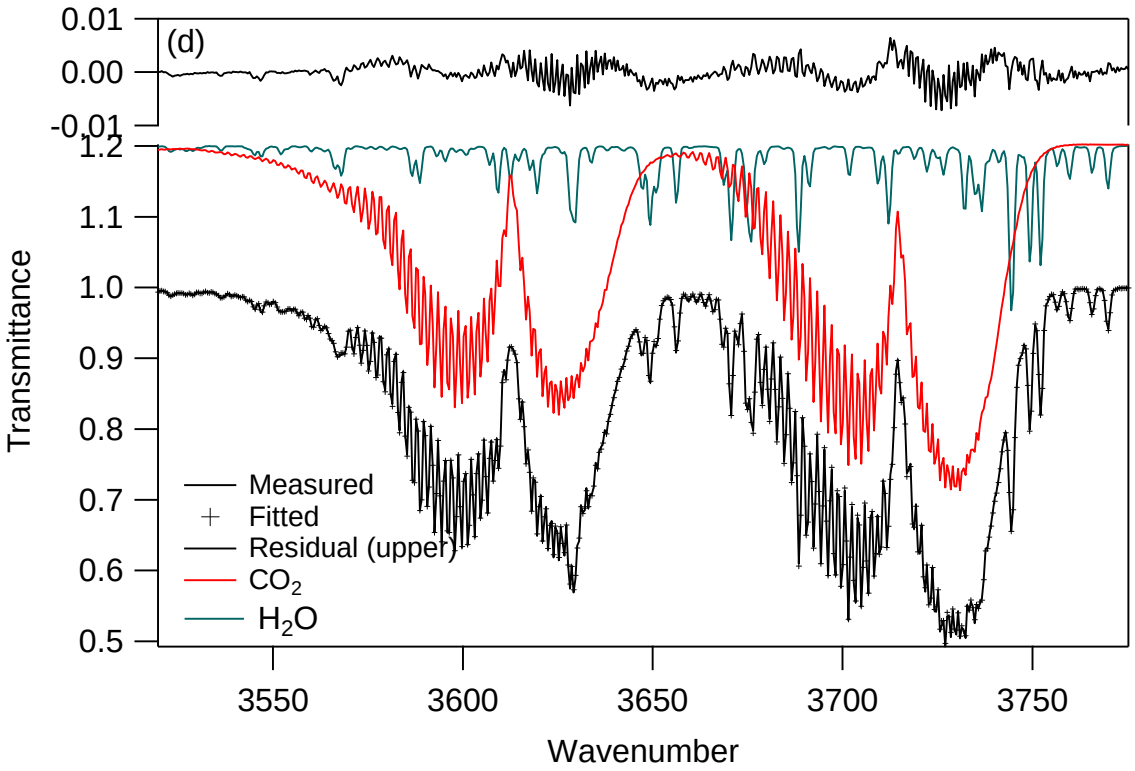

924

925 Figure 3. Typical non-linear least squares fits to a spectrum of dry air in four spectral regions. (a)
926 2150-2310 cm-1, fitting CO2 isotopologues, CO, N2O and H2O; (b) 2097 – 2242 cm-1,
927 optimised for N2O and CO, also fitting CO2; (c) 3001 – 3150 cm-1, fitting CH4 and H2O; (d)
928 3520-3775 cm-1, fitting CO2 and H2O. Contributions from individual species are shown in
929 colours, offset +0.2 units for clarity.

930

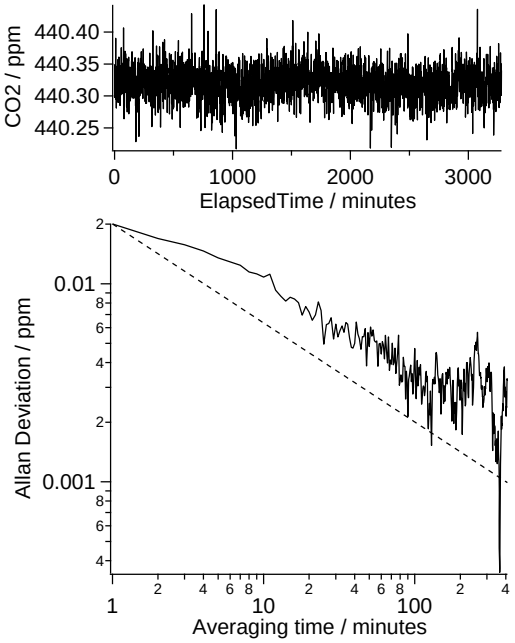
CO2 / ppm
440.40
440.35
440.30
440.25
0
1000
2000
3000
ElapsedTime / minutes
Allan Deviation / ppm
0.01
0.001
1
10
100
Averaging time / minutes

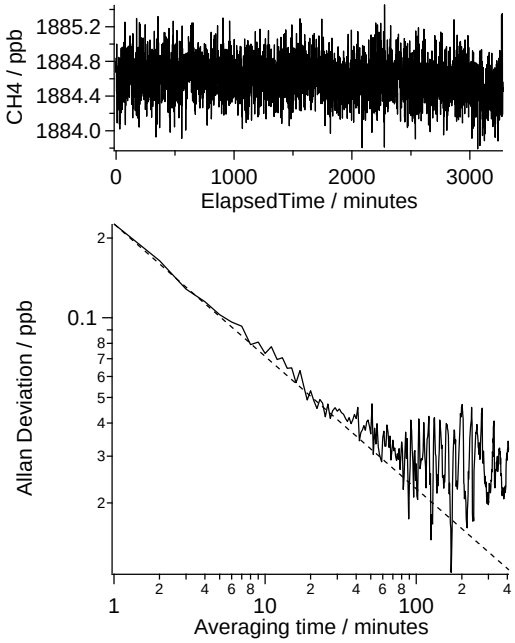
CH4 / ppb
1885.2
1884.8
1884.4
1884.0
0
1000
2000
3000
ElapsedTime / minutes
Allan Deviation / ppb
0.1
1
10
100
Averaging time / minutes

931

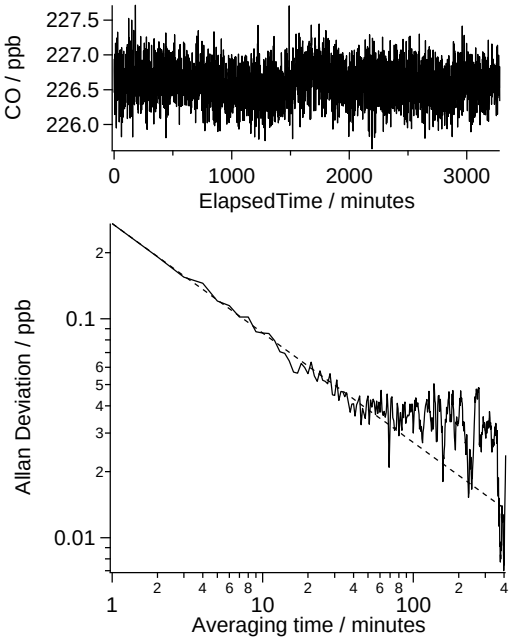
CO / ppb
227.5
227.0
226.5
226.0
0
1000
2000
3000
ElapsedTime / minutes
Allan Deviation / ppb
0.1
0.01
1
10
100
Averaging time / minutes

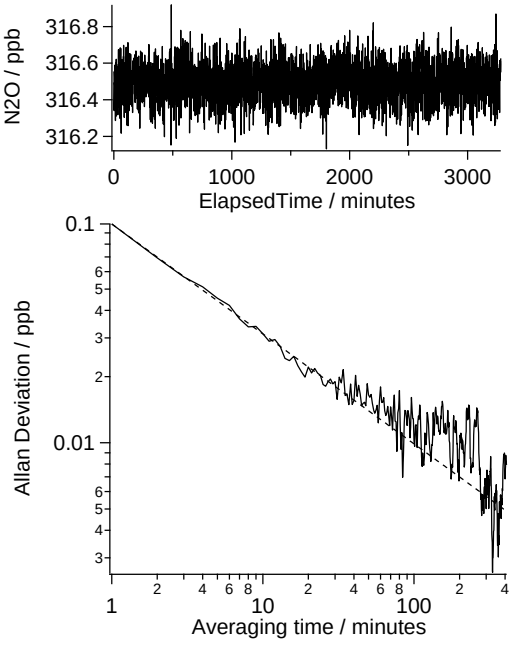
N2O / ppb
316.8
316.6
316.4
316.2
0
1000
2000
3000
ElapsedTime / minutes
Allan Deviation / ppb
0.1
0.01
1
10
100
Averaging time / minutes

932

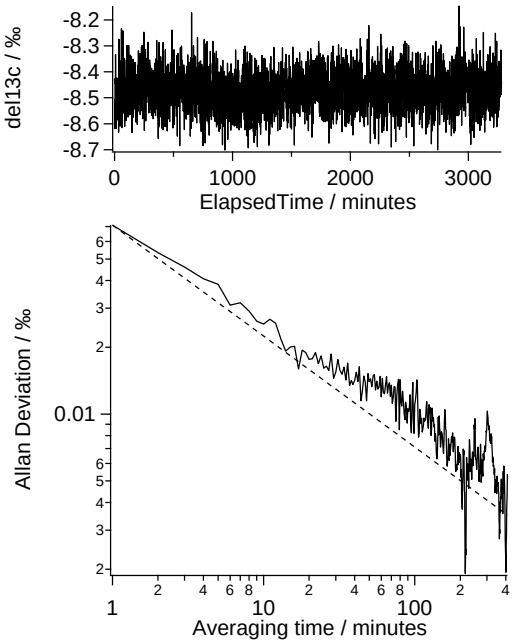

933

934 Figure 4. Time series (upper panels) and Allan deviation (lower panels) plots of consecutive 1-
935 minute average measurements of CO2, CH4, CO, N2O αvδ □13C in CO2 for an unchanging air
936 sample in the FTIR analyser.

937

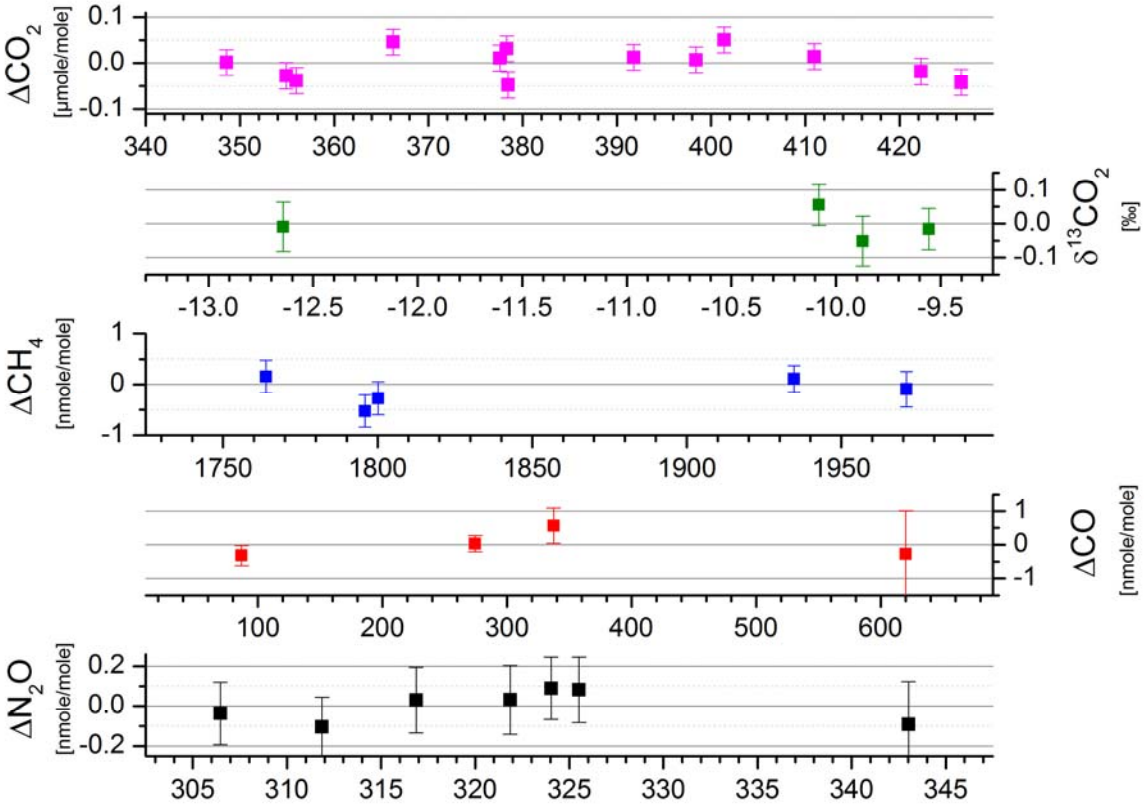

938

939

940 Figure 5. Residuals with 1s error bars from linear regressions of raw FTIR measured mole
941 fractions against reference mole fractions for a suite of tanks maintained by the University of
942 Heidelberg. (Data and further details from Hammer et al. (2012))

943

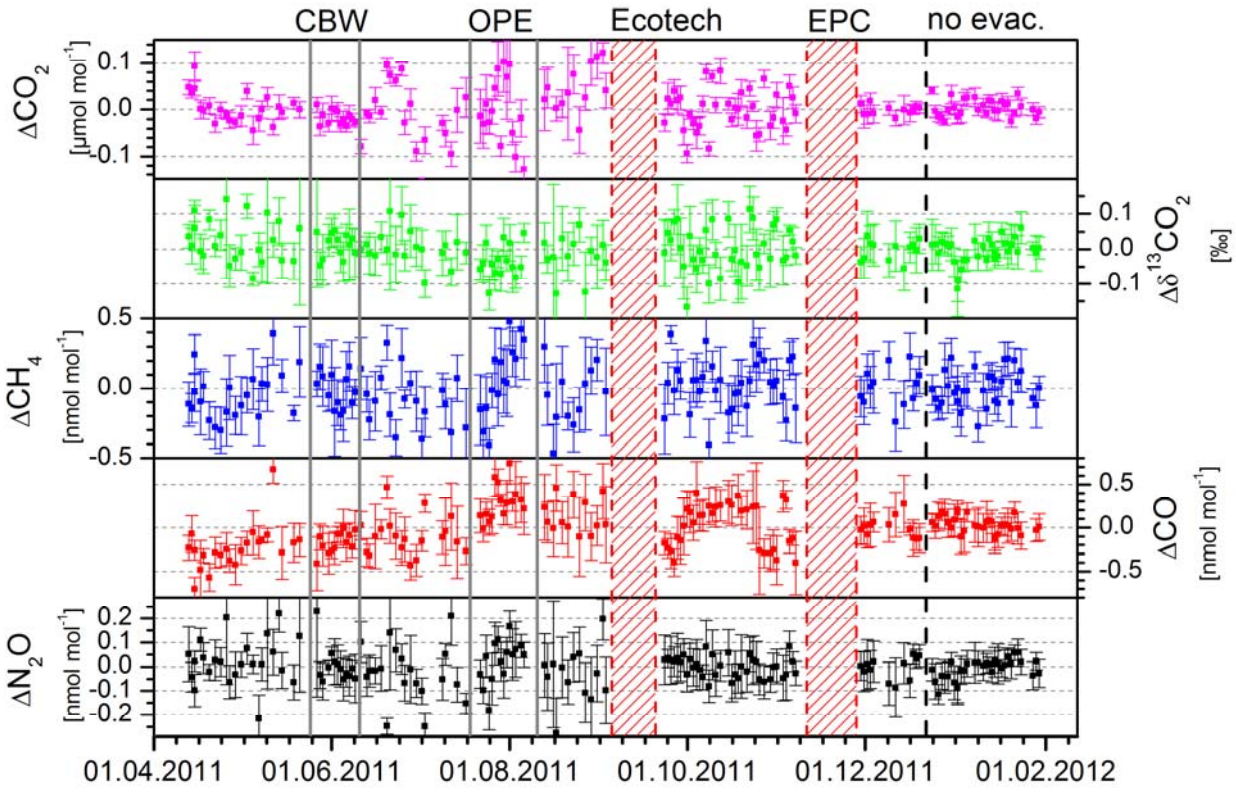

944

945 Figure 6. Measurement residuals with 1s error bars relative to a reference value for a single
946 target tank over a 10 month period (from Hammer et al., 2012). During this period, the FTIR
947 analyser was based in Heidelberg except for two field campaigns at Cabauw, Netherlands
948 (CBW) and Houdelaincourt, France (OPE). "Ecotech" refers to a rebuild of the instrument to
949 include the mass flow controller (section 2) and "EPC" refers to the addition of an electronic
950 pressure controller upstream of the analyser in the sample airstream. "No evac" refers to a period
951 where ambient and target gas in the cell was exchanged by switching flow alone, without
952 evacuation of the cell.

953

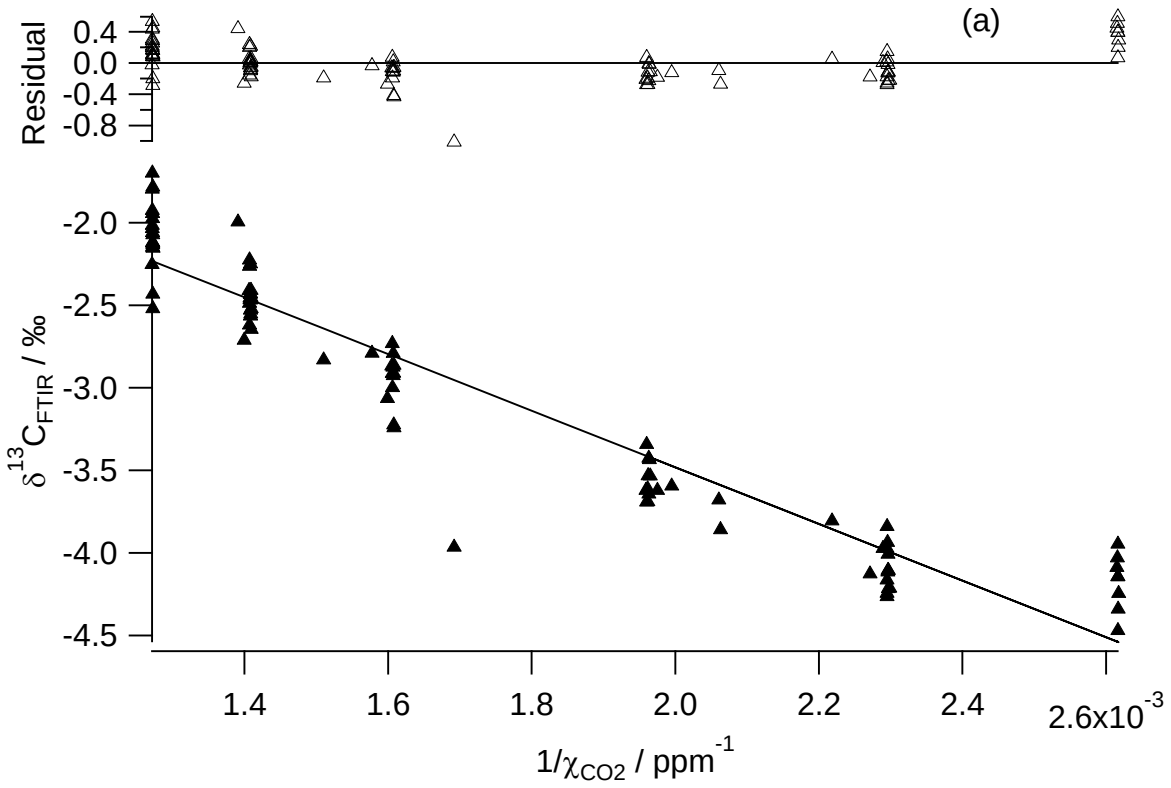

954

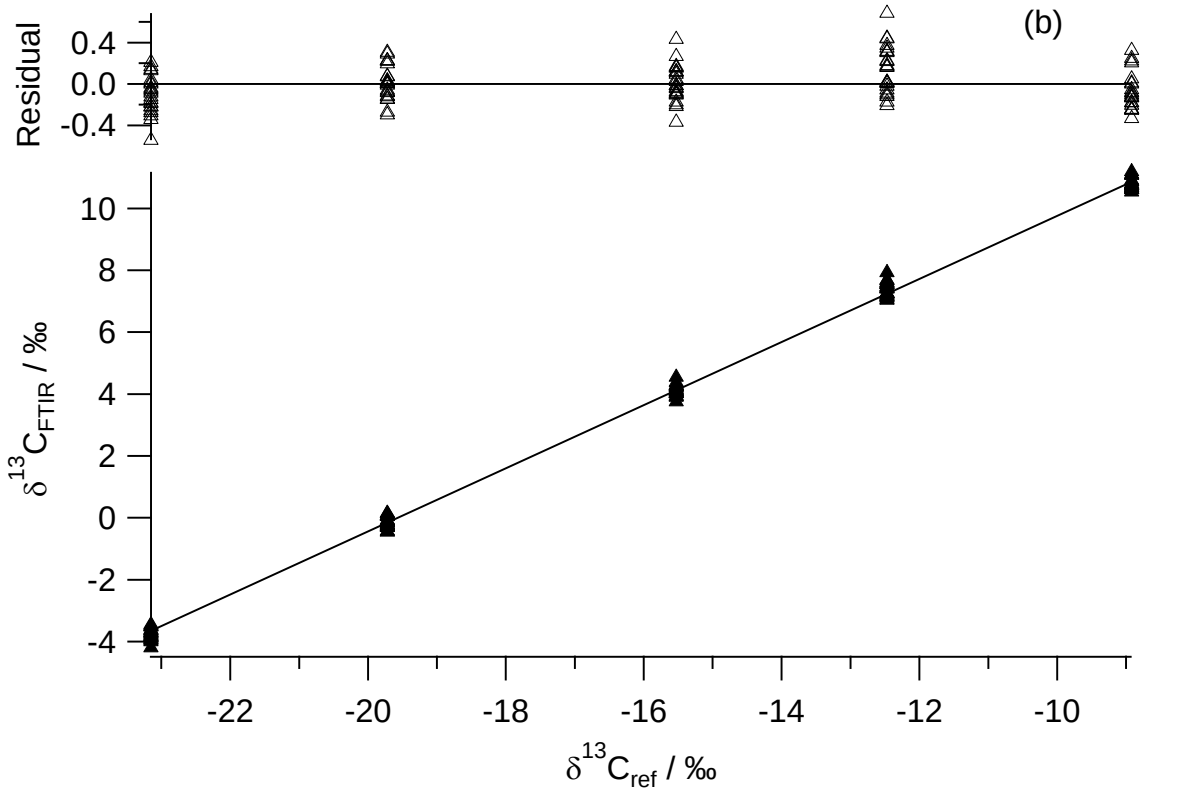

955

956 Figure 7. (a) Empirical dependence of raw measured δ^{13C} in CO2 on the inverse CO2 mole
957 fraction, $1/\chi_{CO2}$, following Eq. (14). Each point is from a 1 minute average spectrum measured
958 during the stepwise stripping sequence from 800 to 330 □mol mol-1 CO2. (b) Fit of Eq. (13) to
959 □13C measured [by] FTIR and corrected for CO2 dependence (see text) against reference values

960 ϕορ five reference tanks with CO2 mole fractions 350-800 □mol mol-1 and □13C values -8 το
961 -23‰. Each point is from a 1-minute average spectrum after filling the measurement cell with
962 reference gas.

963

964

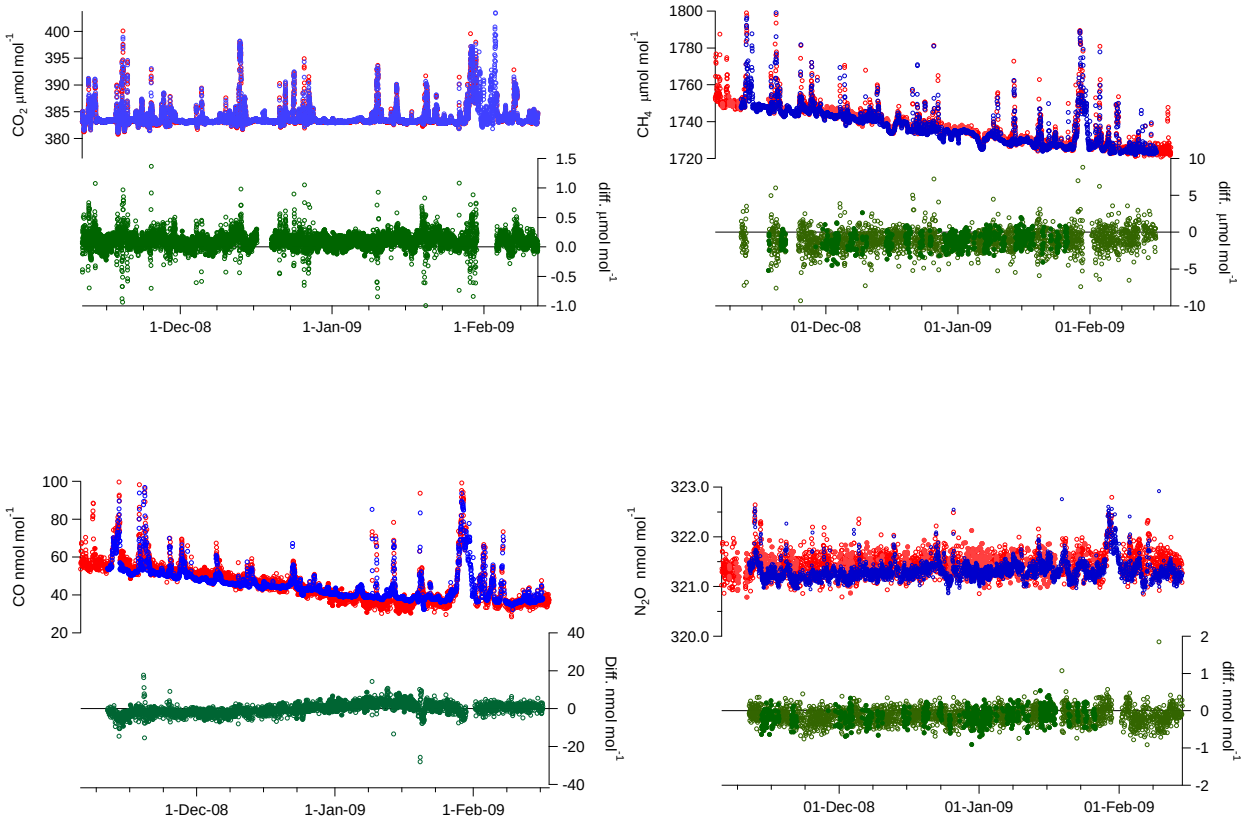

965

966

967

968 Figure 8. Comparisons of FTIR measurements over a 3-month campaign at Cape Grim with
969 LoFlo (CO2) and AGAGE (CH4, CO, N2O) GC measurements. Red: LoFlo/AGAGE. Blue:
970 FTIR. Upper panels: time-coincident measurements. Lower panels: difference. Full circles
971 represent baseline air periods, open circles non-baseline conditions.

972

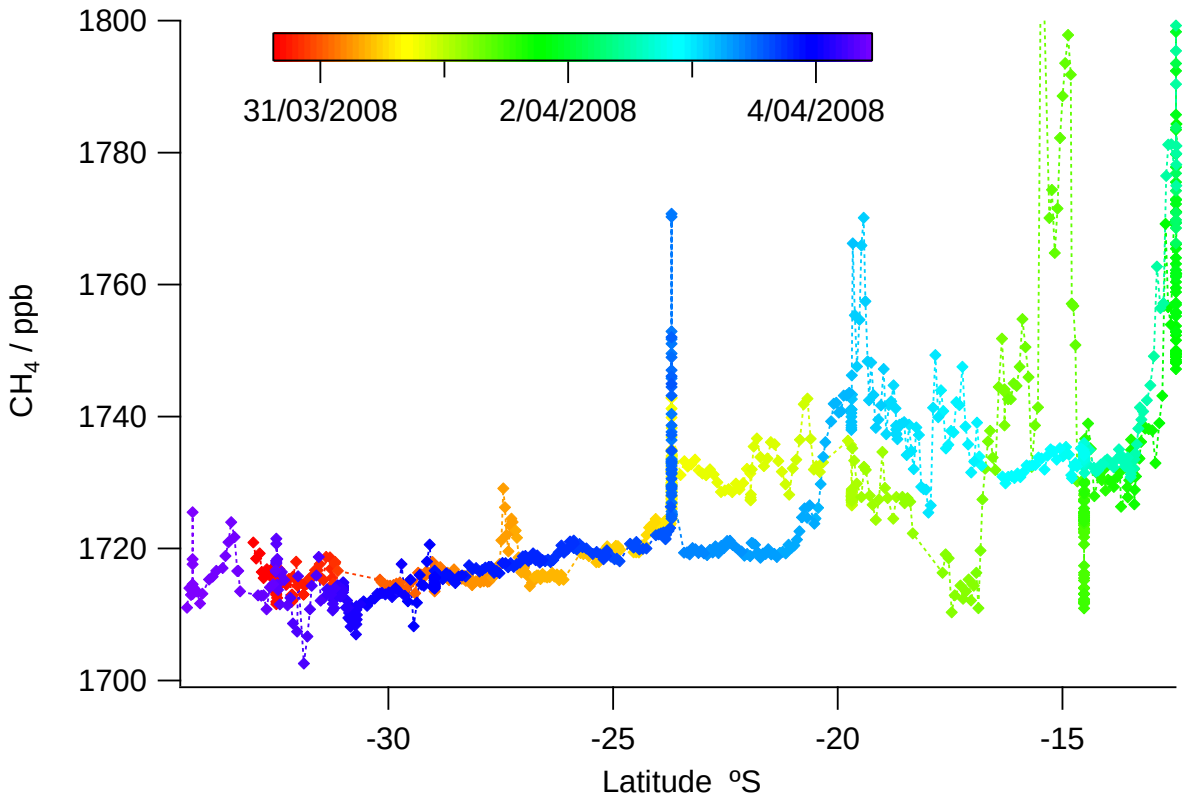

973

974 Figure 9. Measurements of CH_4 along a N-S transect aboard the Ghan train from Adelaide (34ºS)
975 to Darwin (12ºS), March-April 2008.

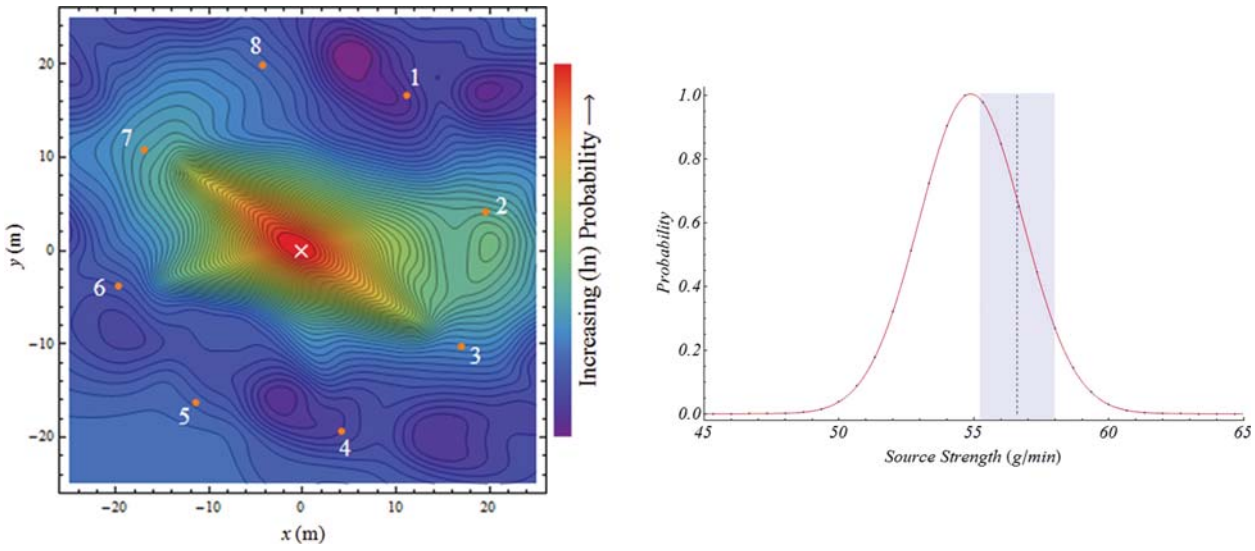

976

977 Figure 10. Result of the FTIR-tomography detection of a CO2 point source release in a 50 x 50
978 m area. In the left hand frame x marks the actual point location (0, 0 m) from where CO2 and
979 N2O were released, and 1-8 mark the locations of the sampling points for the FTIR analyser. The
980 contours plot the a posteriori probability for the source point location determined from the
981 atmospheric measurements (-0.5, 0.5 m). The right hand plot shows the known release rate (56.7
982 ± 0.8 g min-1) and the a posterior probability determined from the measurements (54.9 ± 4 (1□)
983 g min-1). Figure from Humphries et al. (2012), Figure 5.

984

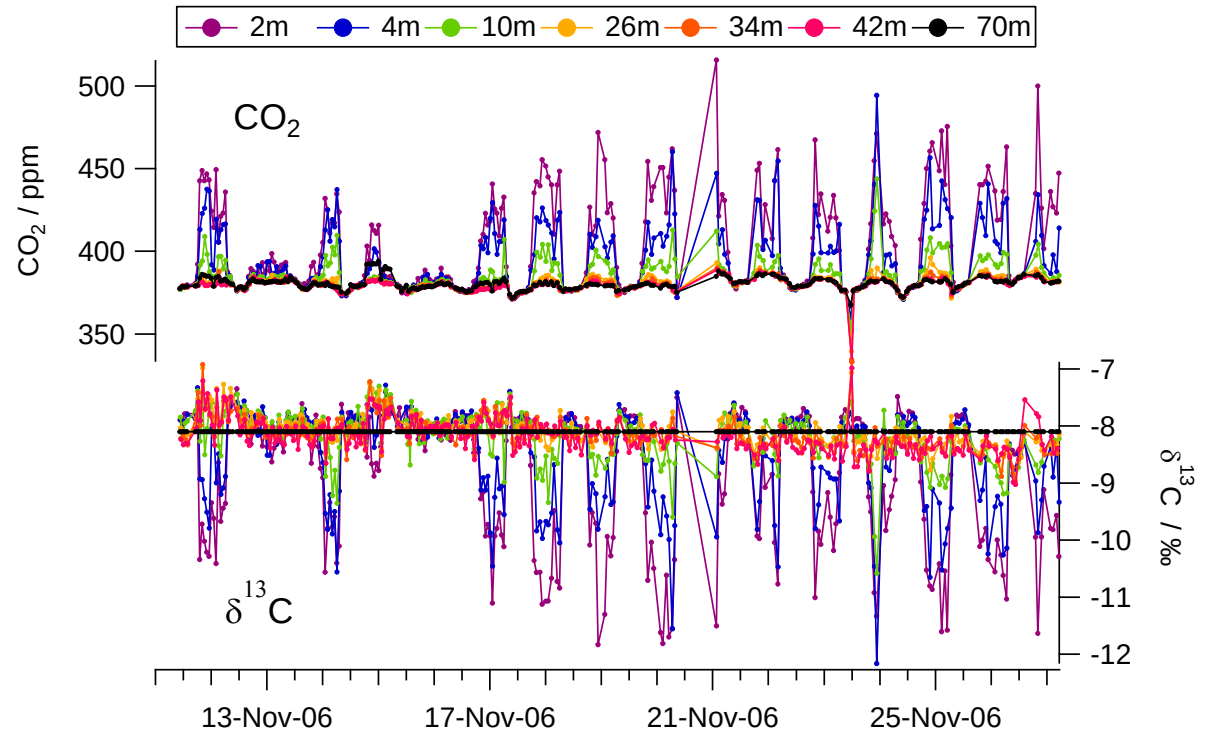

985

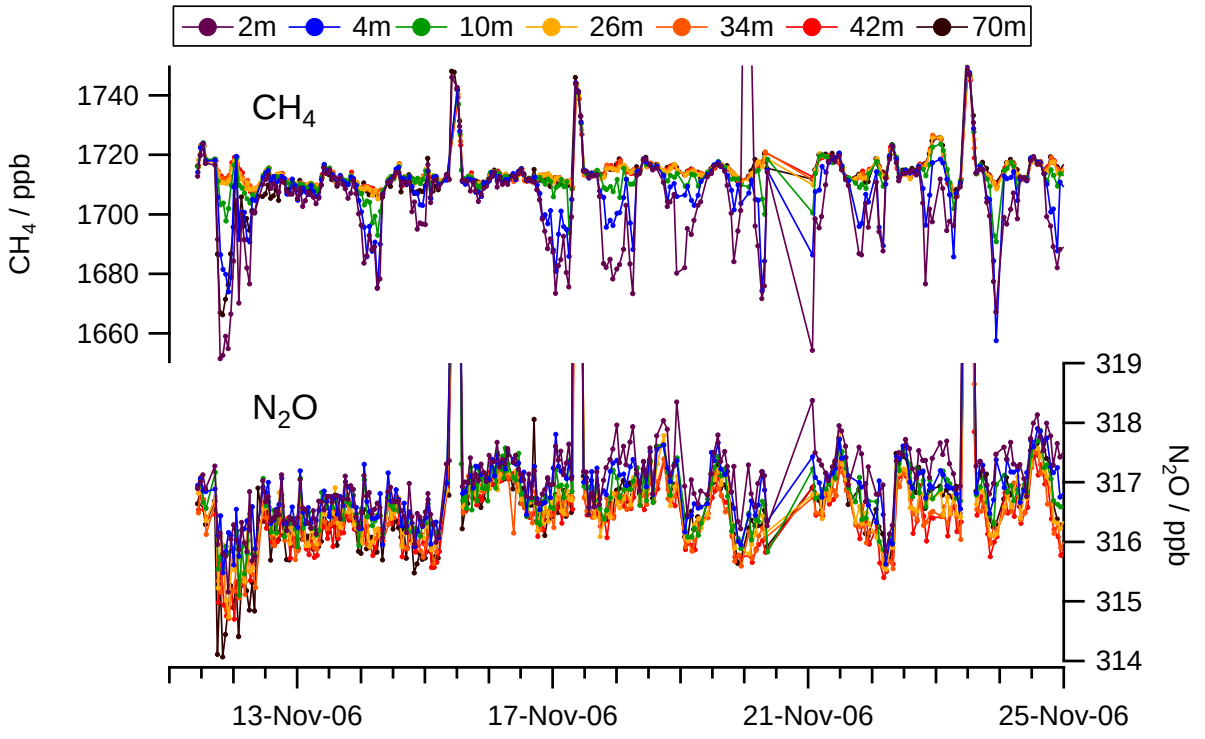

986

987

988 Figure 11. Time series of trace gas mole fractions and δ^{13C} in CO2 during a 3-week campaign at
989 the Ozflux tower site near Tumbarumba, SE Australia in Nov 2006. Seven-point vertical
990 profiles of each species from 2 – 70 m were measured every 30 minutes; colours represent

991 measurements at heights above the surface shown in the legend. The top of the forest canopy is
992 approx 40m above the surface.
993

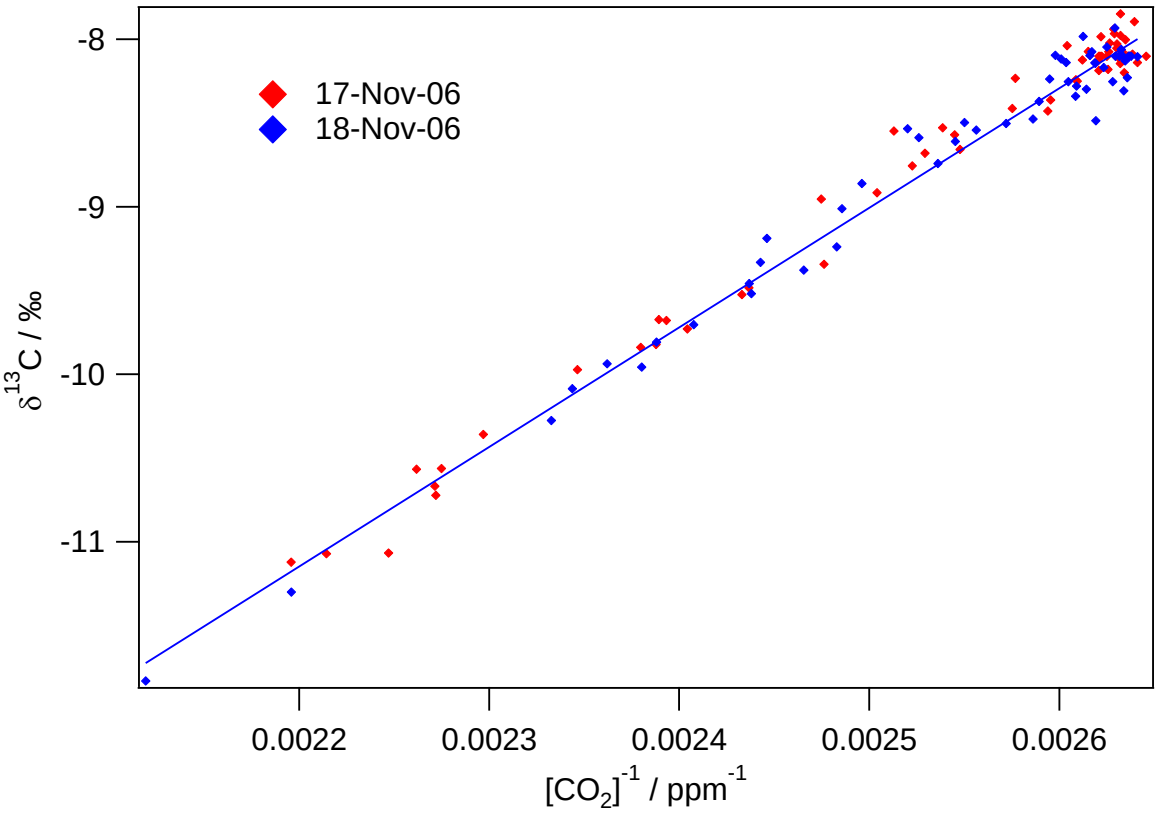

994

995 Figure 12. Keeling plot of δ^{13C} vs 1/[CO2] for two nights drawn from the data shown in Figure
996 11. The mean intercept is -26.8‰, indicative of respiration from the dominant C3 plants in the
997 forest.

998

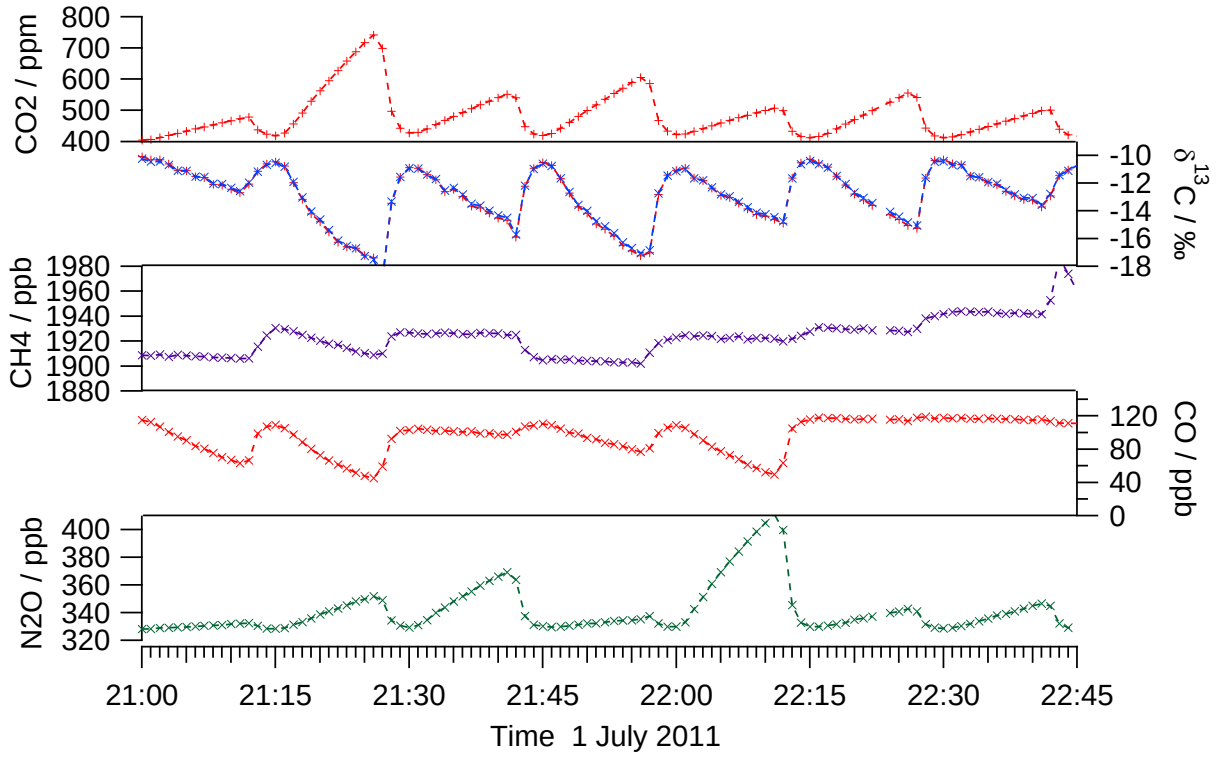

999

1000

1001 Figure 13. Time sequence of mole fractions of CO_2, CH_4, N_2O, CO and $\delta^{13}C$ in CO_2

1002 measurements from seven sequential chamber closures in the Quasom experiment, 1 July 2011.

1003

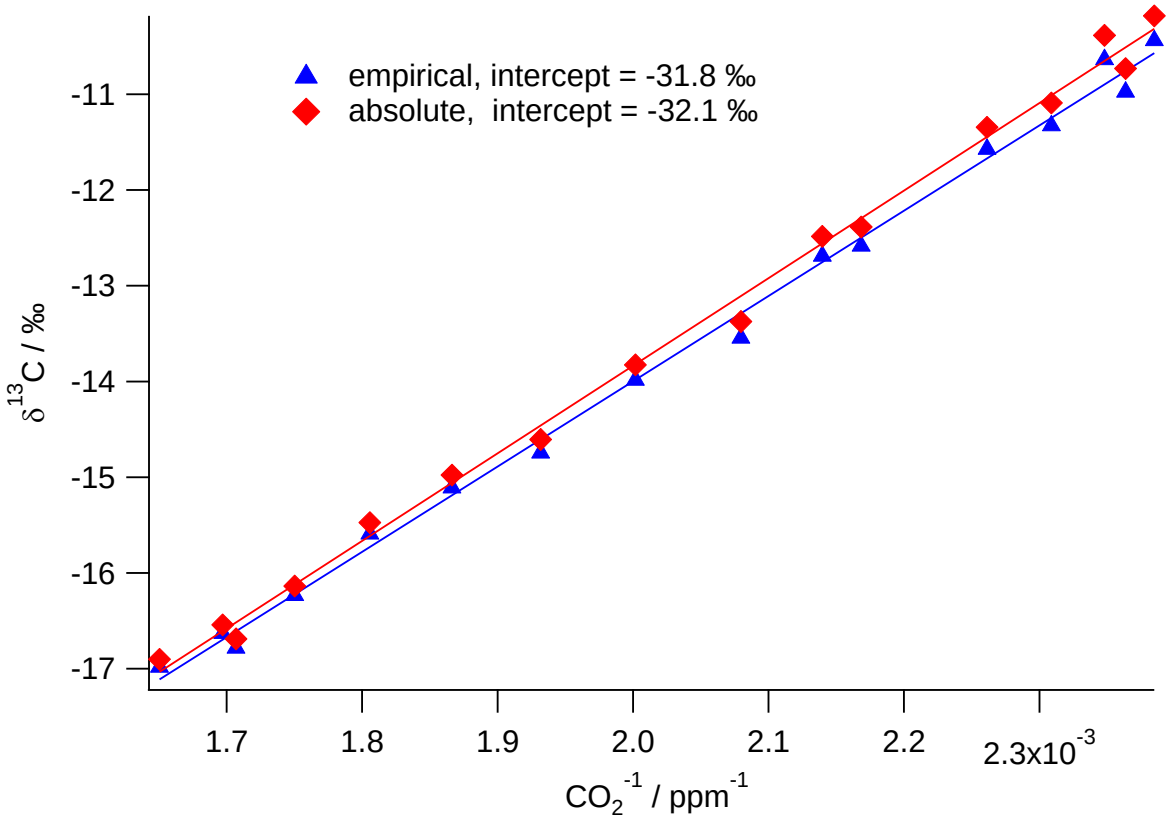

1004

1005 Figure 14. Keeling plot of δ^{13C} vs $1/\chi_{CO2}$ for a typical single chamber closure from the data of
1006 Figure 13. The two plots are derived ^{from} the absolute and empirical □13C calibration methods
1007 described in section 3.

1008

1009

1010

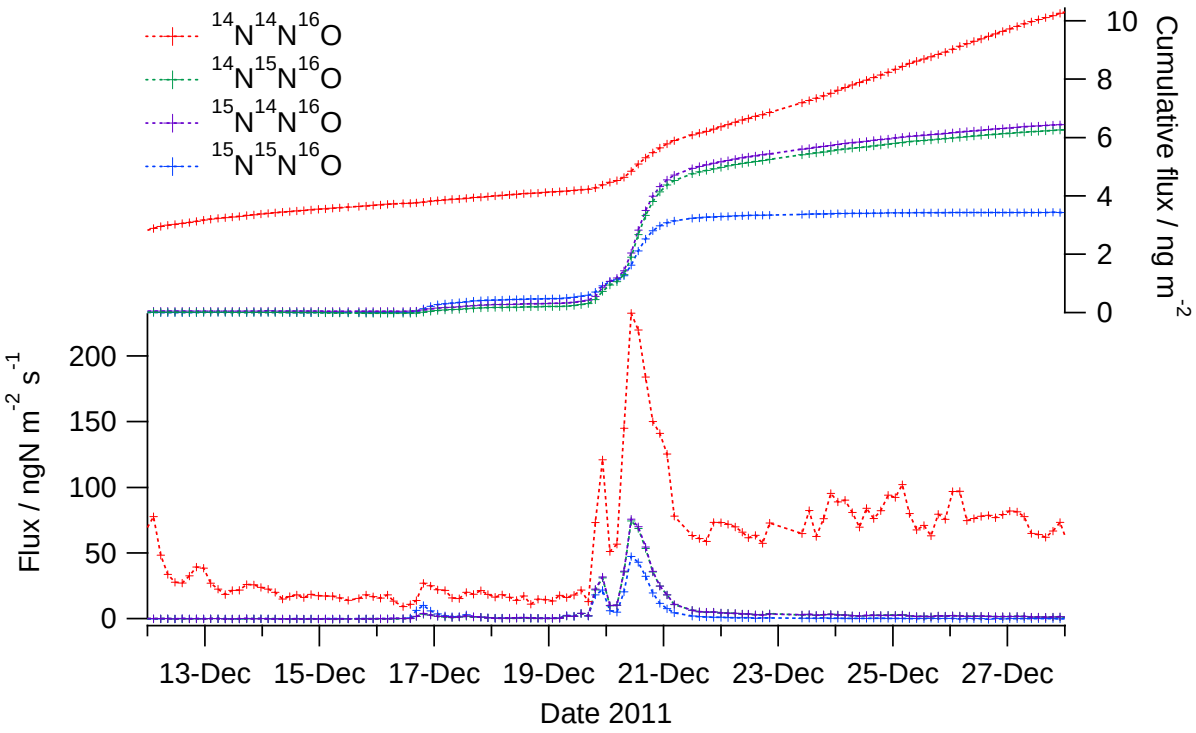

1011

1012

1013 Figure 15. N_2O isotopologue emissions from pasture before and after addition of ^{15}N as nitrate to
1014 the soil on 17 Dec 2011. Approximately 25mm of rainfall fell on 20-21 Dec 2011.

1015